

Unveiling the Significance of Toddler-Inspired Reward Transition in Goal-Oriented Reinforcement Learning

Junseok Park¹, Yoonsung Kim^{1*}, Hee Bin Yoo^{1*}, Min Whoo Lee¹, Kibeom Kim¹, Won-Seok Choi¹,
Minsu Lee^{1,2†}, Byoung-Tak Zhang^{1,2,†}

¹Seoul National University

²AI Institute of Seoul National University (AIIS)

{jspark, yskim, hbyoo, mwlee, kbkim, wchoi, mslee, btzhang}@bi.snu.ac.kr

Abstract

Toddlers evolve from free exploration with sparse feedback to exploiting prior experiences for goal-directed learning with denser rewards. Drawing inspiration from this **Toddler-Inspired Reward Transition**, we set out to explore the implications of varying reward transitions when incorporated into Reinforcement Learning (RL) tasks. Central to our inquiry is the transition from sparse to potential-based dense rewards, which share optimal strategies regardless of reward changes. Through various experiments, including those in egocentric navigation and robotic arm manipulation tasks, we found that proper reward transitions significantly influence sample efficiency and success rates. Of particular note is the efficacy of the toddler-inspired Sparse-to-Dense (S2D) transition. Beyond these performance metrics, using *Cross-Density Visualizer* technique, we observed that transitions, especially the S2D, smooth the policy loss landscape, promoting wide minima that enhance generalization in RL models.

Introduction

In early years, toddlers behave much like exploratory agents. Throughout their development, they interact with their surroundings without much prior knowledge, akin to someone embarking on new experiences without expecting immediate rewards (Oudeyer and Smith 2016). As they grow, toddlers transition from free exploration to more goal-directed learning, aiming for specific goals, resembling someone working towards known rewards for their efforts (Gopnik, Meltzoff, and Kuhl 1999; Gibson 1988; Piaget, Cook et al. 1952; Gopnik et al. 2017) as illustrated in Figure 1.

This learning pattern in toddlers can be incorporated in Reinforcement Learning (RL), as illustrated in Figure 1-(a). In RL, agents learn by interacting with their environment and receiving feedback, much like how toddlers learn from their interactions. Similar to toddlers, agents must navigate towards positive feedback they receive, which can be infrequent (sparse) or detailed (dense). Sparse feedback might mean that the agent requires more attempts to figure out the desired behavior due to limited guidelines (Andrychowicz et al. 2020; Knox et al. 2023). Meanwhile, dense feedback

can guide the agent faster but might inadvertently focus them on immediate outcomes, missing out on the bigger picture or long-term strategies (Laud 2004).

Given these intricacies, simply sticking to one type of feedback might not capture the essence of learning. Drawing inspiration from toddler developmental stages, blending both feedback types could provide richer insights. The transition toddlers make from free exploration – akin to sparse feedback – to specific, goal-driven learning – similar to dense feedback in RL – offers a unique perspective, as shown in Figure 1-(a). With this perspective, our paper addresses the following question: “*How does reward transition that proceeds in a sparse-to-dense manner, inspired by toddler learning, affect the learning of agents?*” Through a series of experiments, including egocentric navigation and robotic arm manipulation tasks, we aim to explore the **Toddler-Inspired Sparse to Potential-based Dense (S2D) Reward Transition**. Our goal is not only to explore its efficacy but also to delve into the underpinning reasons by analyzing its comparative advantages against other rewards or prevalent strategies in the field of RL.

Taking the concept of “reward transition in learning” further, we consider visualizing the learning parameters as a topographical map. One type of such landscape representation, a policy loss landscape provides an intuitive visualization of learning dynamics in RL (Li et al. 2018). On this map, each point corresponds to a set of learning parameters, and its altitude signifies the loss value. As in any landscape, some areas are rugged, featuring steep mountains or deep valleys, indicating challenging learning regions. Understanding the notion of smoothness of loss landscape is vital in neural network-based learning. Smooth terrains in this landscape, devoid of abrupt pitfalls, enable quicker and more reliable convergence through gradient descent.

Critically, smoother landscapes often promote wide minima, which are associated with better generalization of learned policies to novel situations in dynamic environments (Keskar et al. 2017). Empirically, we observed that employing the Sparse-to-Dense (S2D) Reward Transition made this terrain smoother by reducing the depth of local minima, as illustrated in Figure 1-(b).

Our study contributes to a deeper understanding of the intricate balance between exploration and exploitation and provides insight into designing reward structures in RL.

*Equal Contributions.

†Corresponding Authors.

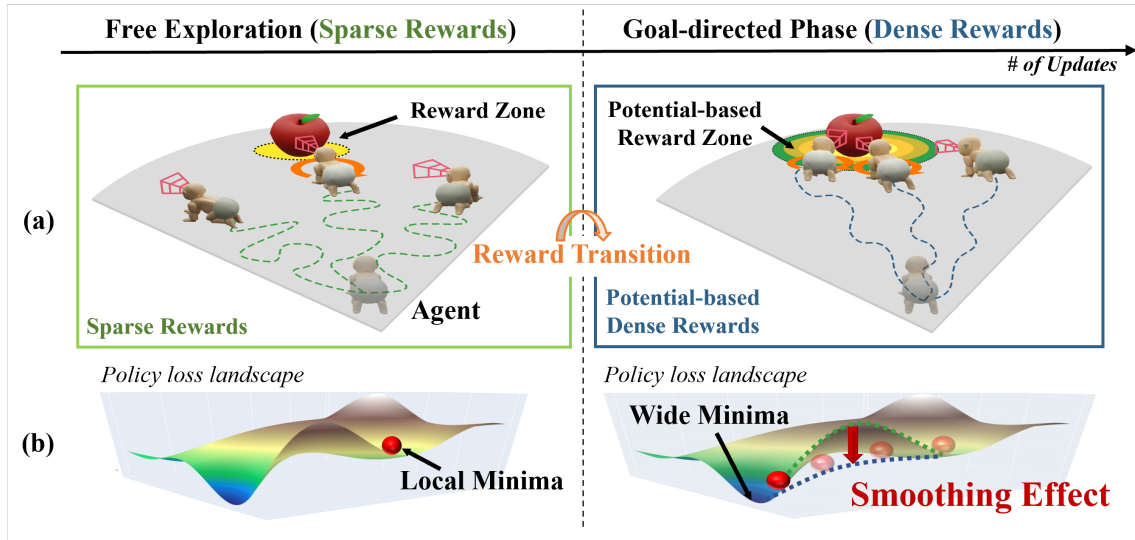


Figure 1: Parallel learning trajectories: toddlers and agents. (a) The figure compares a toddler’s learning journey with an agent’s. On the left, a toddler freely explores the apple, symbolizing sparse reward learning. As we transition right, the toddler’s focus on specific tasks reflects goal-guided learning. Similarly, the agent’s progression from sparse to potential-based dense rewards is charted above, highlighting parallels in learning evolution. (b) As reward transitions occur, the depth of local minima reduces, leading to a wide minima via the smoothing effect, thereby enhancing more generalization.

By emulating the learning processes observed in toddlers, we hope to bridge the gap between biological and artificial learning mechanisms. Based on this, we have offered a novel perspective in applying and addressing this synthesis for more robust, adaptable, and efficient RL systems.

The main contributions of this paper can be summarized as follows: (1) We observed that the Toddler-Inspired Reward Transition enhances success rates, sample efficiency, and generalization within goal-conditioned RL. (2) Our experimental analyses support that such transition has smoothing effects on the policy loss landscape and promotes wide minima, corroborating the performance improvements. (3) Our findings highlight the potential of biologically inspired approaches in providing clues for exploration-exploitation tradeoff and reward shaping challenges.

Related Work

Toddler-inspired learning. Drawing insights from toddler developmental stages has provided a fresh perspective in advancing deep learning. By harnessing the innate exploratory tendencies and distinctive learning mechanisms of toddlers, researchers have refined both supervised and reinforcement learning techniques. For instance, classifiers trained on datasets of toddlers’ perspectives on objects outperformed those using adults’ perspectives (Bam-bach et al. 2018), underscoring the potential of leveraging toddlers’ exploration mechanism. Similarly, critical learning phases in toddlers have counterparts in RL (Park et al. 2021; De Kleijn, Sen, and Kachergis 2022) and deep networks (Achille, Rovere, and Soatto 2018). Such toddler-inspired methodologies emphasize the alignment between toddler growth and AI model evolution, underscoring the po-

tential of biological insights in driving AI forward.

Exploration-exploitation in deep RL. Balancing exploration with exploitation is an inherent challenge of RL (Lad-osz et al. 2022). Moreover, deep RL intensifies this complexity with high-dimensional spaces, like raw image inputs, where pixels are unique dimensions. To mitigate this, many algorithms favor exploration, utilizing tools like intrinsic motivation (Badia et al. 2020; Aubret, Matignon, and Hassas 2019; Pathak et al. 2017). Drawing from toddlers’ learning, we observe the transition from free exploration to specific exploitation based on collected previous experience. Our approach offers a fresh take on RL’s exploration-exploitation dilemma without introducing algorithmic complexities.

Curriculum learning. Curriculum Learning (CL), inspired by curricula in human’s education, has been known to boost performance, training speed (Hacohen and Weinshall 2019), and safety (Turchetta et al. 2020) in machine learning. CL’s progression from simple to complex tasks promotes generalization and convergence (Bengio et al. 2009; Weinshall, Cohen, and Amir 2018) in both supervised and reinforcement learning (Florensa et al. 2018; Graves et al. 2017; Narvekar and Stone 2020). Unlike the studies that initially restrict the diversity to easy tasks (Kalantidis et al. 2020; Du et al. 2021; Dong, Gong, and Zhu 2017), several studies (Zhang 1994; MacKay 1992) advocate a *general-to-specific* approach, where agent initially collects varied learning experiences and then exploits these experiences later in the curriculum. Adapting the S2D transition observed in toddlers into RL, we embrace this philosophy in reward transition for goal-oriented tasks.

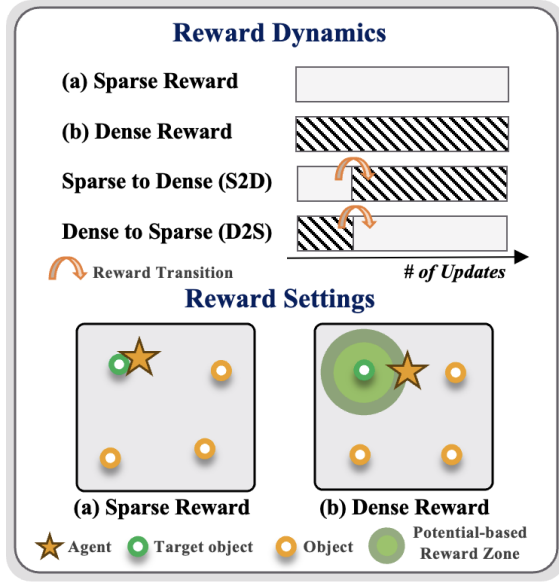


Figure 2: Overview of the baseline rewards. The S2D presents reward inspired by toddler learning. In sparse rewards, agents are rewarded upon reaching the target. For potential-based dense rewards, they get an extra reward determined by the distance to a specific unit from the object.

Potential-based reward shaping (PBRS). In RL, maximizing cumulative rewards guides agent behavior. However, due to the inherent challenges in designing optimal reward functions for various tasks, it often necessitates a process known as reward engineering. Reward Shaping (RS) is one such technique that enhances training by supplementing the environment’s feedback (Taylor and Stone 2009). Particularly, in environments where the reward changes, an additional reward from a *potential function* is employed to ensure the agent’s optimal strategy remains unaffected (Ng, Harada, and Russell 1999b). Commonly, such shaped rewards are consistently applied throughout training. Unlike this, we explore the **Toddler-Inspired Reward Transition**, focusing on the effects of changing the density of rewards.

Preliminaries

Reinforcement learning. RL is a field of machine learning in which the agent learns through trial and error, similar to how humans acquire skills. It is applied to various tasks that involve sequential decision making. A widely used formulation of RL problem, Markov Decision Process (MDP) is defined as $\langle \mathcal{S}, \mathcal{A}, \mathcal{P}, \mathcal{R}, \gamma \rangle$, where \mathcal{S} is a set of environment states, \mathcal{A} is a set of possible actions, $\mathcal{P} : \mathcal{S} \times \mathcal{A} \rightarrow \Delta(\mathcal{S})$ is a transition probability distribution, $\mathcal{R} : \mathcal{S} \times \mathcal{A} \rightarrow \mathbb{R}$ is a reward function and γ is a discount factor. At every time step $t \in \mathbb{N}$, the agent in the current state $s_t \in \mathcal{S}$ performs the action $a_t \in \mathcal{A}$ according to a policy $\pi(\cdot|s_t)$, and receives the next state $s_{t+1} \sim \mathcal{P}(\cdot|s_t, a_t)$ and reward $\mathcal{R}(s_t, a_t)$. RL algorithms aim to obtain an optimal policy $\pi^* \in \Pi^*$ that maximizes the expected cumulative rewards $R = \mathbb{E} [\sum_{t=0}^{\infty} \gamma^t \mathcal{R}(s_t, a_t)]$ with γ applied, where Π^* is the

set of optimal policies.

Curriculum learning. Curriculum Learning (CL) is a strategy to train an ML model using tasks that gradually increase in difficulty. In RL, CL can be formulated as a learning framework where the agent is trained on a sequentially changing series of MDPs $\mathcal{M}_i = \langle \mathcal{S}, \mathcal{A}, \mathcal{P}, \mathcal{R}_i, \gamma \rangle$.

Definition 1 (Curriculum) Let $\mathcal{M}_1, \mathcal{M}_2, \dots, \mathcal{M}_N$ be a sequence of MDPs $\mathcal{M}_i = \langle \mathcal{S}, \mathcal{A}, \mathcal{P}, \mathcal{R}_i, \gamma \rangle$, and $\mathcal{T} = (T_1, T_2, \dots, T_{N-1}) \in \mathbb{N}^{N-1}$. A curriculum is a tuple $\mathcal{C} = (\{\mathcal{M}_i\}_{i=1}^N, \mathcal{T})$ where the agent is trained on $\mathcal{M}_{I(t; \mathcal{T})}$ at training step t . Stage indicator $I(t; \mathcal{T})$ is defined as:

$$I(t; \mathcal{T}) := i, \quad t \in [T_{i-1}, T_i)$$

for each stage $i \in \{1, \dots, N\}$, where $T_0 := 0$ and $T_N := \infty$. We call $\mathcal{T} = (T_1, T_2, \dots, T_{N-1})$ the stage transitions.

CL also boosts the training by arranging the tasks as “general-to-specific,” where the agent is provided rewards with monotonically increasing densities over training. Formally, we say an environment is sparse when only a small portion of the state space is included in $\text{supp}(\mathcal{R})$. That is,

$$|\text{supp}(\mathcal{R})| \ll |\mathcal{S}|, \quad \text{where}$$

$$\text{supp}(\mathcal{R}) = \{s \in \mathcal{S} \mid \exists a \in \mathcal{A} \text{ s.t. } \mathcal{R}(s, a) \neq 0\}.$$

$\text{supp}(\mathcal{R})$ means the region *supported* by reward function \mathcal{R} which has non-zero reward for some actions.

Wide minima phenomenon and loss landscape. Deep neural networks traverse a high-dimensional *loss landscape*, with altitude indicating the loss for specific parameters (Li et al. 2018). The aim is to find the *minima*. In *wide minima*, due to broad gradients, gradient descent is more likely to converge smoothly to global minima. This fosters robustness and superior generalization to new data (Keskar et al. 2016). Conversely, in *sharp minima*, steep gradients can trap models in local minima, resulting in overfitting and poor generalization across diverse data distributions (Goodfellow, Vinyals, and Saxe 2014). Empirically, models within wide minima demonstrate better performance and generalization than those in sharp minima (Keskar et al. 2017; Jastrzebski et al. 2018). In deep RL as well, where the distribution of agent’s experiences may slightly vary every time step, policies in wide minima could improve in generalization.

Toddler-Inspired Reward Transition

To conduct our experiments, we need to formulate and design a toddler-inspired reward transition in RL, emulating the toddler reward transition paradigm. Furthermore, we analyze the influence of this reward transition on the learning behavior of agents, focusing on the policy loss landscape and the wide minima phenomenon.

Toddler-Inspired Sparse to Potential-based Dense Reward Curriculum

In this paper, we harness curriculum learning from the perspective of encouraging exploration-to-exploitation as a Sparse to potential-based Dense (S2D) reward transition curriculum and explain how this learning mechanism can benefit RL. We define $\mathcal{C} = (\{\mathcal{M}_i\}_{i=1}^N, \mathcal{T})$ as an *S2D-curriculum*

if reward functions of MDPs $(\mathcal{M}_1, \mathcal{M}_2, \dots, \mathcal{M}_N)$ become progressively denser while preserving optimality.

Definition 2 (Toddler-inspired S2D-curriculum) A curriculum $\mathcal{C} = (\{\mathcal{M}_i\}_{i=1}^N, \mathcal{T})$ with MDPs $\{\mathcal{M}_i\}_{i=1}^N$ is an S2D-curriculum if following conditions are satisfied:

$$\text{supp}(\mathcal{R}_1) \subseteq \text{supp}(\mathcal{R}_2) \subseteq \dots \subseteq \text{supp}(\mathcal{R}_N) \quad (1)$$

$$\Pi_1^* \supseteq \Pi_2^* \supseteq \dots \supseteq \Pi_N^*, \quad (2)$$

Π_i^* is a set of optimal policies with MDP \mathcal{M}_i . Here, we call $\{\mathcal{R}_i\}_{i=1}^N$ a guidance of the curriculum \mathcal{C} .

The first condition in Equation 1 denotes that the reward function becomes denser, *i.e.*, the guidance becomes more explicit. The second condition in Equation 2 constrains the optimality to be preserved during the transition of the MDPs, *i.e.*, the optimal policies of \mathcal{M}_i are also optimal in \mathcal{M}_{i+1} . At a high level, the sequence of MDPs in the above definition is S2D-curricular in the sense that the reward functions are arranged in a “sparse-to-dense” order.

Visualizing Post-Transition 3D Policy Loss Landscape: Cross-Density Visualizer

As seen in Figure 6 and Appendix B, our study delves into the effect of the S2D transition on policy loss landscape, reflecting toddlers’ cognitive evolution (Gopnik et al. 2017; Piaget, Cook et al. 1952). Following (Li et al. 2018), we visualize the policy loss landscapes using grids of parameters $\tilde{\theta} = \theta + \alpha \mathbf{x} + \beta \mathbf{y}$. Here, θ signifies current parameters and α, β are normalized coordinates. Vectors \mathbf{x} and \mathbf{y} that form the axes arise from two specific perturbations in the network’s parameter space. \mathbf{x} and \mathbf{y} are made unit vectors by a normalized filter for consistent scaling and clarity. The Z-axis captures policy loss, averaged over a batch of transitions from the replay buffer. We are not concerned with the altitude and which landscape is above or below another, because the two landscapes correspond to separate network parameters, each of them having its own loss range according to its current learning progress.

Noting the lack of visualization techniques in prior studies for policy loss landscapes based on reward transitions, we design the Cross-Density Visualizer. This method portrays the 3D policy loss landscape during transitions from purely sparse or dense rewards to mixed-reward settings. Thus, one set includes Sparse-to-Dense (S2D) and Sparse-to-Sparse (Only Sparse), while the other contains Dense-to-Sparse (D2S) and Dense-to-Dense (Only Dense). Our representations, displayed in Figure 6 and expanded upon in Appendix B, highlight comparable *smoothing effects* particularly in the S2D model.

Exploring Minima Sharpness After Reward Transitions

Observing a reduction in the depth of local minima due to smoothing effects led us to hypothesize that the S2D transition promotes escape from local minima and enhances generalization in wide minima. Wide minima in neural networks can serve as a measure indicating robust and adaptable models (Keskar et al. 2017; Jastrzębski et al. 2018). By exploring

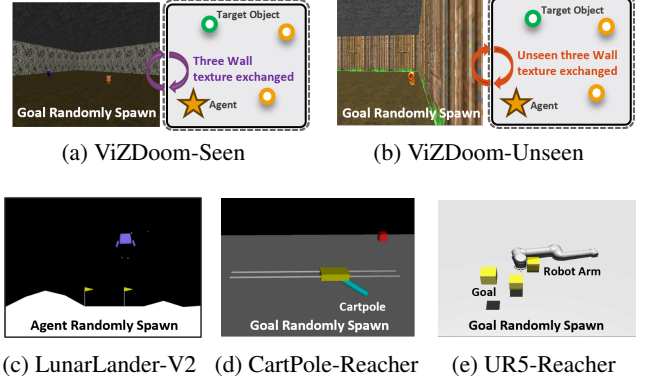


Figure 3: Experimental environments. In particular, (a) and (b) are environments for evaluating generalization.

minima with this transition, we aspire for both performance and a deeper grasp of agent adaptability in diverse scenarios. To check how much the policy resides in a wide minima, we measure the end-of-training convergence of S2D’s neural network to wide minima using the sharpness metric of Equation 3 and compare with those of baselines in the same way as proposed in (Foret et al. 2021), which is a specific form of sharpness measure proposed in (Keskar et al. 2017).

$$\max_{\|\epsilon\|_2 \leq \rho} L_\pi(\theta + \epsilon) - L_\pi(\theta) \quad (3)$$

Here, θ is the current parameter in the policy loss landscape. The maximizer ϵ can be estimated from $\hat{\epsilon} = \rho \text{sgn}(\nabla_\theta L_\pi(\theta)) \cdot |\nabla_\theta L_\pi(\theta)|^{q-1} / (|\nabla_\theta L_\pi(\theta)|^q)^{\frac{1}{p}}$, where $1/p + 1/q = 1$, $\text{sgn}(\cdot)$ is element-wise sign function (Foret et al. 2021). We use $\rho = 0.02, p = 2$ in our experiments.

Experiments

In our experimental section, we delve deeply into the dynamics of the S2D reward transition compared to multiple reward-driven methods. We unveil its substantial effects within multiple challenging environments, which are illustrated in Appendix A. We particularly explored the implications of applying the reward transition to RL by probing three critical questions:

- **Performance Enhancement:** How does the Toddler-inspired S2D reward transition compare to other diverse reward settings?
- **Post-Transition 3D Policy Loss Landscape:** What are the effects of the S2D transition on the policy loss landscape?
- **Correlation Between Wide Minima and Toddler-Inspired Reward Transition:** Does the S2D transition foster convergence to wide minima?

Our understanding is further supported by extensive supplementary experiments in Appendix C.

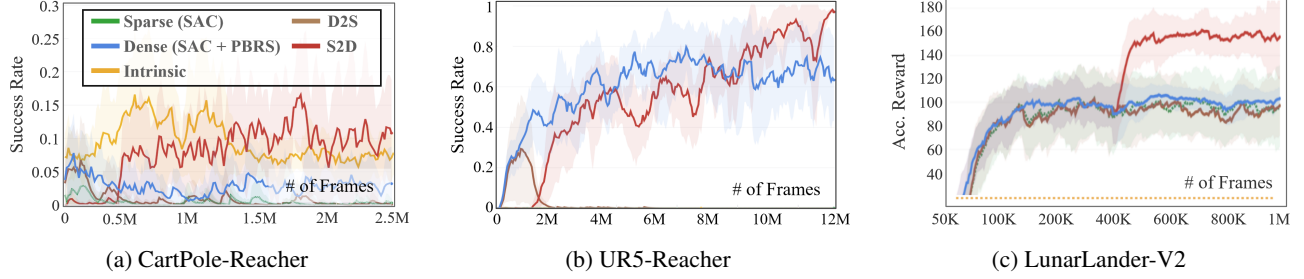


Figure 4: Performance of the agent with various reward types in multiple goal-oriented tasks. Notably, in (c) LunarLander, the accumulated reward from intrinsic rewards was significantly below zero, indicated by a dashed line.

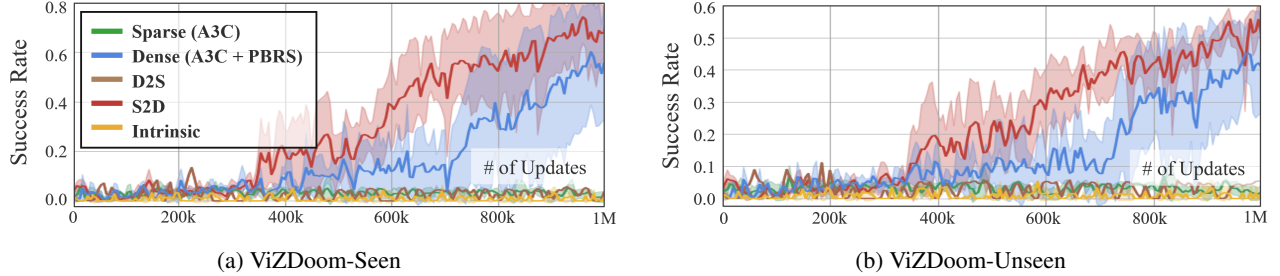


Figure 5: Generalization performance of the ViZDoom agent with various types of rewards.

Reward Setting Details

Design of sparse and dense reward. In the sparse reward setting, the agent receives a reward only upon success, i.e., when reaching the goal. In the dense reward setting, the agent receives a potential-based reward based on its proximity to the goal. This is expressed as $\psi(s) = \text{diam}(\mathcal{S}) - \|s - g\|_2$, where \mathcal{S} is the set of states, $g \in \mathcal{S}$ is the goal state, and $\text{diam}(\cdot)$ denotes the diameter of the given set.

Reward-driven baselines for comparison. Aiming to investigate the relation between exploration-exploitation tradeoff and reward transitions, we explore the Sparse-to-Dense (S2D) approach to mirror toddlers’ developmental progression. We also evaluate its counterpart, Dense-to-Sparse (D2S), and solely sparse or dense reward schemes for a comprehensive assessment of reward strategies. Given the prominence of intrinsic motivation in tackling exploration-exploitation, we adopted NGU (Badia et al. 2020)—designed for discrete environments like ViZDoom and LunarLander—and RND (Burda et al. 2018)—tailored for continuous action such as CartPole and UR5—as additional baselines. Both methods incentivize agents to explore by providing additional intrinsic rewards for discovering novel states.

Design for reward transition. We also explored the hyperparameter for reward transition through ablation studies as seen in Table 1. Recognizing the importance of the temporal aspects of initial cognitive and motor interactions in early developmental stages (Piaget, Cook et al. 1952; Shonkoff and Phillips 2000), we divide the first quarter and seg-

mented this period into three points for reward transition. We set the transition timings at $t \in \{1N, 2N, 3N\}$, where N corresponds to roughly a third of the first quarter of the entire training duration. The specific value of N , adjusted for each environment’s episode length, is detailed in the Appendix A. We denote these phases as \mathcal{C}_1 , \mathcal{C}_2 , and \mathcal{C}_3 , signifying the S2D or D2S reward transition points.

Environment Details

We assess the efficacy of reward dynamics across diverse conditions, encompassing state and visual observations as well as both discrete and continuous action domains, as seen in Appendix A. We evaluate the reward settings, including S2D reward transition, across a variety of goal-based tasks in well-established benchmark environments. As seen in Figure 3, these include LunarLander (Brockman et al. 2016), CartPole, and UR5 (Todorov, Erez, and Tassa 2012). In Appendix A, we particularly detail challenging dynamics for UR5 and CartPole, featuring randomized placements of the agent, goal, and obstacles, termed the ‘reacher’ version. All agents have full access to the current state and are tested using the SAC (Haarnoja et al. 2018) algorithm. We also adjusted the reward structure for both sparse and dense settings, with details in Appendix A.

Environment for generalization. To measure the improvement in generalization, we design a challenging egocentric navigation task using the ViZDoom environment (Kempka et al. 2016), depicted in Figure 3. In the **Seen** environment (Appendix Figure 9-(a)), object locations

Task	Metric	S2D(\mathcal{C}_1)	S2D(\mathcal{C}_2)	S2D(\mathcal{C}_3)	Only Sparse	Only dense	D2S(\mathcal{C}_1)	D2S(\mathcal{C}_2)	D2S(\mathcal{C}_3)
Lunar Lander	Perf.	138.71 \pm 3.71	63.40 \pm 160.55	168.88 \pm 23.66	142.50 \pm 4.25	139.68 \pm 14.90	140.75 \pm 7.46	130.63 \pm 19.69	142.373 \pm 15.62
	Sharp.	27.06 \pm 36.31	1231.93 \pm 2424.61	7.46 \pm 3.37	8.97 \pm 2.83	8.71 \pm 4.43	8.95 \pm 2.89	8.99 \pm 2.97	11.32 \pm 3.72
CartPole	Perf.	3.18 \pm 4.0	14.61 \pm 10.96	5.29 \pm 7.472	0.14 \pm 0.25	3.88 \pm 4.63	1.55 \pm 0.29	0.38 \pm 0.07	0.97 \pm 0.19
	Sharp.	0.12 \pm 0.24	0.01 \pm 0.15	0.01 \pm 0.24	0.08 \pm 0.57	0.19 \pm 0.03	0.16 \pm 0.09	0.05 \pm 0.21	0.02 \pm 0.17
UR5	Perf.	65.54 \pm 10.86	65.69 \pm 17.32	94.15 \pm 4.28	0.00 \pm 0.00	64.23 \pm 13.03	0.00 \pm 0.00	0.00 \pm 0.00	0.00 \pm 0.00
	Sharp.	0.67 \pm 0.01	0.62 \pm 0.11	0.61 \pm 0.04	0.09 \pm 0.52	0.67 \pm 0.01	0.52 \pm 0.24	0.56 \pm 0.28	0.47 \pm 0.20

Table 1: Performance and sharpness metric measured for more than 5 different random seeds in each environment. We highlight the best performance and its sharpness values in bold, confirming that the top-performing S2D also resides in the widest minima.

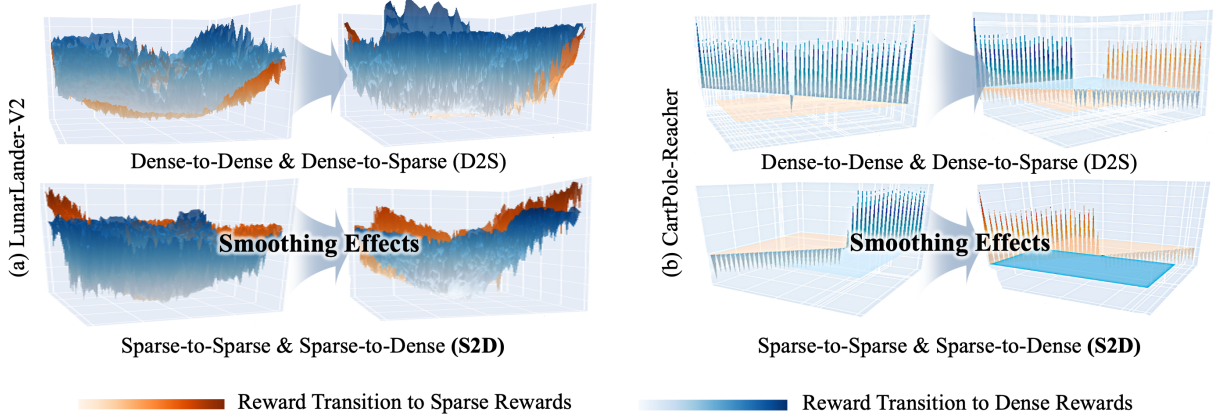


Figure 6: The 3D visualization illustrates the policy loss landscape following a reward transition, which begins with either a sparse or dense reward. It includes two sets of transitions: one transitioning from sparse-to-dense (S2D) and to sparse (Only Sparse), and the other from dense-to-dense (Only Dense) and to sparse (D2S). Notably, the S2D transitions often exhibited more distinct smoothing effects locally compared to others. These effects were noticeable after the transition at T=50 and T=2000 in LunarLander, and at T=3500 in Cartpole. Detailed 3D visualizations for environments are available in Appendix B.

are random, and walls have one of three textures. The **Unseen** environment (Appendix Figure 9-(b)) requires generalization to three new wall textures, distinct from the **Seen** environment. Here, We employed A3C (Mnih et al. 2016).

Results

Performance Enhancement

Sample efficiency and success rate. Experiments are conducted in diverse environments with sparse rewards, and the results are shown in Figure 4, 5 and Table 1. The agents in LunarLander, CartPole-Reacher, ViZDoom-Seen, and ViZDoom-Unseen environments achieve the lowest performance with default sparse rewards. S2D consistently outperforms all other baselines in these settings, achieving better sample efficiency. Even in UR5-Reacher, which is notably more challenging with only sparse rewards than in other environments, the S2D strategy consistently outperforms other baselines. While algorithms based on intrinsic motivation often prioritized exploration over goal attainment in goal-oriented RL tasks, our approach exhibited exceptional results, exhibiting better exploration-exploitation tradeoff while being simple and universally applicable. Importantly, the outcomes associated with D2S consistently fall below those of S2D across all environments, underlin-

ing the efficacy of the S2D transition as a curriculum.

Generalization performance. The S2D reward transition outperforms other agents across all dynamic environments requiring generalization as seen in Figure 5-(a), (b). Particularly in ViZDoom-Unseen, where agents encounter drastic visual changes with the emergence of three previously unseen walls, the S2D transition achieves robust generalization and superior performance compared to other baselines.

Post-Transition 3D Policy Loss Landscape

We note a marked smoothing effect at various update points after the reward transition, attributed to the reduction in the depth of local minima, as shown in Table 2 and Figure 6. This effect is predominantly observed under the S2D reward. Such smoothing could aid in overcoming local minima, possibly leading to wide minima. 3D policy loss landscapes of other reward baselines are visualized using the Cross-Density Visualizer in Appendix B. To further verify the smoothing quantitatively, we calculate the depth of local minima of π_θ function, which measures the average of differences between the local maximum and minimum values for a number of updates after the reward transition. The results, as shown in Table 2, demonstrate that the depth primarily decreased for the S2D reward transition model.

Task	Reward Transition	Number of updates after reward transition								
		phase \mathcal{P}_1	$\Delta\mathcal{P}_1$	phase \mathcal{P}_2	$\Delta\mathcal{P}_2$	phase \mathcal{P}_3	$\Delta\mathcal{P}_3$	phase \mathcal{P}_4	$\Delta\mathcal{P}_4$	phase \mathcal{P}_5
Lunar Lander	S2D(\mathcal{C}_3)	0.031 \pm 0.01	-0.004	0.027\pm0.01	+0.003	0.030\pm0.01	-0.008	0.022\pm0.00	-0.001	0.021\pm0.00
	D2S(\mathcal{C}_3)	0.043 \pm 0.02	-0.008	0.035 \pm 0.00	+0.004	0.039 \pm 0.01	+0.004	0.043 \pm 0.02	-0.009	0.034 \pm 0.01
	only sparse	0.029\pm0.01	0.000	0.029 \pm 0.00	+0.005	0.034 \pm 0.01	-0.004	0.030 \pm 0.00	+0.007	0.037 \pm 0.01
	only dense	0.039 \pm 0.01	-0.007	0.032 \pm 0.01	0.000	0.032 \pm 0.01	+0.005	0.037 \pm 0.01	-0.002	0.035 \pm 0.01
CartPole	S2D(\mathcal{C}_2)	0.028 \pm 0.00	+0.003	0.031\pm0.01	0.000	0.031\pm0.00	+0.005	0.036\pm0.00	-0.013	0.023\pm0.00
	D2S(\mathcal{C}_2)	0.033 \pm 0.01	+0.014	0.047 \pm 0.04	+0.001	0.048 \pm 0.01	-0.002	0.046 \pm 0.02	+0.001	0.047 \pm 0.02
	only sparse	0.027\pm0.01	+0.016	0.043 \pm 0.01	-0.009	0.034 \pm 0.01	+0.007	0.041 \pm 0.02	-0.014	0.027 \pm 0.00
	only dense	0.033 \pm 0.01	+0.021	0.054 \pm 0.02	-0.013	0.041 \pm 0.02	+0.004	0.045 \pm 0.02	-0.001	0.044 \pm 0.01
UR5	S2D(\mathcal{C}_3)	0.084 \pm 0.01	+0.016	0.100 \pm 0.02	-0.033	0.067 \pm 0.01	+0.028	0.095 \pm 0.02	-0.062	0.033\pm0.01
	D2S(\mathcal{C}_3)	0.060 \pm 0.03	-0.007	0.053 \pm 0.02	-0.005	0.048 \pm 0.02	+0.011	0.059 \pm 0.02	-0.003	0.056 \pm 0.01
	only sparse	0.059\pm0.02	-0.013	0.046\pm0.00	0.000	0.046\pm0.01	+0.031	0.077 \pm 0.00	-0.031	0.046 \pm 0.01
	only dense	0.079 \pm 0.02	-0.012	0.067 \pm 0.02	-0.009	0.058 \pm 0.02	-0.005	0.053\pm0.01	+0.005	0.058 \pm 0.01

Table 2: Comparison of the depth of local minima in policy loss following reward transitions. A lower depth of local minima indicates a smoother terrain. Phase \mathcal{P}_i indicates the number of updates, which are ($T = 50, 400, 800, 1200, 1600$) for LunarLander, and ($T = 50, 1000, 2000, 3000, 4000$) for others.

Results of Wide Minima

We assess the end-of-training convergence of the neural networks guided by S2D using sharpness metrics and contrast this with the baselines. Areas of lower sharpness correspond to wide minima, which can enhance generalization performance. As demonstrated in Table 1, only the agents guided by S2D reward transition that converge to the widest minima exhibit superior performance in challenging environments.

Discussion and Analyses

In the following analyses, we clearly address the three pivotal questions raised in our experimental framework:

Performance enhancement. As shown in Figure 4, Figure 5, and Table 1, S2D surpassed other reward baselines. In our experiments comparing intrinsic motivation methods, we observed that agents driven by such algorithms tend to prioritize state coverage over achieving specific goals in goal-oriented RL tasks. This suggests that while they may excel in exploration, the S2D transition approach more effectively balances exploration and exploitation, thus ensuring proper goal acquisition. Additionally, we explored the optimal timing for reward transition through ablation studies. While this timing is unique for each environment, it was, in all cases, near a quarter of the total training time. Particularly challenging tasks like UR5-Reacher required longer periods of free exploration compared to relatively simpler ones, such as LunarLander. This echoes the critical early learning phases observed in infants.

Post-transition 3D policy loss landscape. Our 3D visualizations reveal that S2D predominantly smooths the landscape. Although our main experiments are based on SAC, we also tested other algorithms such as PPO (Schulman et al. 2017) and DQN (Mnih et al. 2013) for more comprehensive analyses. This smoothing effect was also uniquely seen with the S2D reward transition in additional gridworld experiments, as discussed in Appendix C.

In UR5, minima depth for S2D decreased significantly from 0.095 to 0.033 in phase \mathcal{P}_5 . This may relate to its higher performance than only dense rewards particularly at a later stage, as in Figure 4-(b). Conversely, in CartPole and LunarLander, performance quickly improved after the reward transition, reflecting S2D’s overall low local minima.

Correlation between wide minima and toddler-inspired reward transition. In Table 1, S2D-guided agents converged to the widest minima with the highest performance in the LunarLander and CartPole-Reacher, where agents receiving only sparse rewards achieved nonzero performance. Conversely, in the UR5-Reacher, agents with only sparse rewards showed zero performance. This implies that in sparse reward situations, premature convergence into wide minima can lead to gradient stagnation and retain low sharpness, with high variance. Yet, S2D, compared to only dense rewards, still posts the highest performance with the lowest sharpness, suggesting its alignment within wide minima.

Conclusion

Inspired by toddler developmental learning, our research pioneers a shift from static, single-density to dynamic reward transitions in goal-oriented RL. This toddler-inspired approach demonstrates notable effects of transitions on learning dynamics in RL. We examine its implications across various scenarios, focusing on its efficiency. Using the Cross-Density Visualizer, we observe the primary smoothing effects on the policy loss landscape during the S2D transition. Sharpness metrics further confirm the smoothing effects of S2D, guiding agents towards wider minima to improve generalization. This blend of biological and artificial paradigms may lead to robust, high-performance learning systems.

Limitations. While our study focuses on understanding the implications of S2D reward transition, we haven’t provided an automatic method for finding an optimal transition yet. Nonetheless, our preliminary research on criteria sets the stage for future development of automated methods.

Acknowledgments

The authors would like to express their sincere gratitude to Inwoo Hwang, Changhoon Jeong, Moonhoen Lee, and Dong-Sig Han for their insightful discussions and valuable suggestions on the early drafts of this paper. This work was partly supported by the IITP (2021-0-02068-AIHUB/15%, 2021-0-01343-GSAI/10%, 2022-0-00951-LBA/15%, 2022-0-00953-PICA/25%) and NRF (RS-2023-00274280/10%, 2021R1A2C1010970/25%) grant funded by the Korean government.

References

- Achille, A.; Rovere, M.; and Soatto, S. 2018. Critical learning periods in deep networks. In *International Conference on Learning Representations*.
- Andrychowicz, O. M.; Baker, B.; Chociej, M.; Jozefowicz, R.; McGrew, B.; Pachocki, J.; Petron, A.; Plappert, M.; Powell, G.; Ray, A.; et al. 2020. Learning dexterous in-hand manipulation. *The International Journal of Robotics Research*, 39(1): 3–20.
- Aubret, A.; Matignon, L.; and Hassas, S. 2019. A survey on intrinsic motivation in reinforcement learning. *arXiv preprint arXiv:1908.06976*.
- Badia, A. P.; Sprechmann, P.; Vitvitskyi, A.; Guo, D.; Piot, B.; Kapturowski, S.; Tieleman, O.; Arjovsky, M.; Pritzel, A.; Bolt, A.; et al. 2020. Never give up: Learning directed exploration strategies. *arXiv preprint arXiv:2002.06038*.
- Bambach, S.; Crandall, D.; Smith, L.; and Yu, C. 2018. Toddler-inspired visual object learning. *Advances in neural information processing systems*, 31.
- Bengio, Y.; Louradour, J.; Collobert, R.; and Weston, J. 2009. Curriculum learning. In *ICML '09*.
- Brockman, G.; Cheung, V.; Pettersson, L.; Schneider, J.; Schulman, J.; Tang, J.; and Zaremba, W. 2016. Openai gym. *arXiv preprint arXiv:1606.01540*.
- Burda, Y.; Edwards, H.; Storkey, A.; and Klimov, O. 2018. Exploration by random network distillation. *arXiv preprint arXiv:1810.12894*.
- De Kleijn, R.; Sen, D.; and Kachergis, G. 2022. A Critical Period for Robust Curriculum-Based Deep Reinforcement Learning of Sequential Action in a Robot Arm. *Topics in Cognitive Science*, 2(2): 311–326.
- Dong, Q.; Gong, S.; and Zhu, X. 2017. Class rectification hard mining for imbalanced deep learning. In *Proceedings of the IEEE International Conference on Computer Vision*, 1851–1860.
- Du, B.; Gao, X.; Hu, W.; and Li, X. 2021. Self-Contrastive Learning with Hard Negative Sampling for Self-Supervised Point Cloud Learning. In *Proceedings of the 29th ACM International Conference on Multimedia*, MM '21, 3133–3142. New York, NY, USA: Association for Computing Machinery. ISBN 9781450386517.
- Florensa, C.; Held, D.; Geng, X.; and Abbeel, P. 2018. Automatic goal generation for reinforcement learning agents. In *International conference on machine learning*, 1515–1528. PMLR.
- Foret, P.; Kleiner, A.; Mobahi, H.; and Neyshabur, B. 2021. Sharpness-aware Minimization for Efficiently Improving Generalization. In *International Conference on Learning Representations*.
- Gibson, E. J. 1988. Exploratory behavior in the development of perceiving, acting, and the acquiring of knowledge. *Annual review of psychology*, 39(1): 1–42.
- Goodfellow, I. J.; Vinyals, O.; and Saxe, A. M. 2014. Qualitatively characterizing neural network optimization problems. *arXiv preprint arXiv:1412.6544*.
- Gopnik, A.; Meltzoff, A. N.; and Kuhl, P. K. 1999. *The scientist in the crib: Minds, brains, and how children learn*. William Morrow & Co.
- Gopnik, A.; O’Grady, S.; Lucas, C. G.; Griffiths, T. L.; Wente, A.; Bridgers, S.; Aboody, R.; Fung, H.; and Dahl, R. E. 2017. Changes in cognitive flexibility and hypothesis search across human life history from childhood to adolescence to adulthood. *Proceedings of the National Academy of Sciences*, 114(30): 7892–7899.
- Graves, A.; Bellemare, M. G.; Menick, J.; Munos, R.; and Kavukcuoglu, K. 2017. Automated curriculum learning for neural networks. In *international conference on machine learning*, 1311–1320. PMLR.
- Haarnoja, T.; Zhou, A.; Abbeel, P.; and Levine, S. 2018. Soft actor-critic: Off-policy maximum entropy deep reinforcement learning with a stochastic actor. In *International conference on machine learning*, 1861–1870. PMLR.
- Hacohen, G.; and Weinshall, D. 2019. On The Power of Curriculum Learning in Training Deep Networks. *ArXiv*, 2.
- Harutyunyan, A.; Devlin, S.; Vrancx, P.; and Nowé, A. 2015. Expressing arbitrary reward functions as potential-based advice. In *Proceedings of the AAAI Conference on Artificial Intelligence*, volume 29.
- Jastrzębski, S.; Kenton, Z.; Arpit, D.; Ballas, N.; Fischer, A.; Bengio, Y.; and Storkey, A. 2018. Finding Flatter Minima with SGD.
- Kalantidis, Y.; Saryildiz, M. B.; Pion, N.; Weinzaepfel, P.; and Larlus, D. 2020. Hard Negative Mixing for Contrastive Learning. In Laroche, H.; Ranzato, M.; Hadsell, R.; Balcan, M.; and Lin, H., eds., *Advances in Neural Information Processing Systems*, volume 33, 21798–21809. Curran Associates, Inc.
- Kempka, M.; Wydmuch, M.; Runc, G.; Toczek, J.; and Jaśkowski, W. 2016. Vizdoom: A doom-based ai research platform for visual reinforcement learning. In *2016 IEEE conference on computational intelligence and games (CIG)*, 1–8. IEEE.
- Keskar, N. S.; Mudigere, D.; Nocedal, J.; Smelyanskiy, M.; and Tang, P. T. P. 2016. On large-batch training for deep learning: Generalization gap and sharp minima. *arXiv preprint arXiv:1609.04836*.
- Keskar, N. S.; Mudigere, D.; Nocedal, J.; Smelyanskiy, M.; and Tang, P. T. P. 2017. On Large-Batch Training for Deep Learning: Generalization Gap and Sharp Minima. In *International Conference on Learning Representations*.

- Kim, K.; Lee, H.; Lee, M. W.; Lee, M.; Lee, M.; and Zhang, B.-T. 2023a. L-SA: Learning Under-Explored Targets in Multi-Target Reinforcement Learning. *arXiv preprint arXiv:2305.13741*.
- Kim, K.; Lee, M. W.; Kim, Y.; Ryu, J.; Lee, M.; and Zhang, B.-T. 2021. Goal-aware cross-entropy for multi-target reinforcement learning. *Advances in Neural Information Processing Systems*, 34: 2783–2795.
- Kim, K.; Shin, K.; Lee, M. W.; Lee, M.; Lee, M.; and Zhang, B.-T. 2023b. Visual Hindsight Self-Imitation Learning for Interactive Navigation. *arXiv preprint arXiv:2312.03446*.
- Knox, W. B.; Allievi, A.; Banzhaf, H.; Schmitt, F.; and Stone, P. 2023. Reward (mis) design for autonomous driving. *Artificial Intelligence*, 316: 103829.
- Ladosz, P.; Weng, L.; Kim, M.; and Oh, H. 2022. Exploration in deep reinforcement learning: A survey. *Information Fusion*, 85: 1–22.
- Laud, A. D. 2004. *Theory and application of reward shaping in reinforcement learning*. University of Illinois at Urbana-Champaign.
- Li, H.; Xu, Z.; Taylor, G.; Studer, C.; and Goldstein, T. 2018. Visualizing the loss landscape of neural nets. *Advances in neural information processing systems*, 31.
- MacKay, D. J. 1992. Information-based objective functions for active data selection. *Neural computation*, 4(4): 590–604.
- Mnih, V.; Badia, A. P.; Mirza, M.; Graves, A.; Lillicrap, T.; Harley, T.; Silver, D.; and Kavukcuoglu, K. 2016. Asynchronous methods for deep reinforcement learning. In *International conference on machine learning*, 1928–1937. PMLR.
- Mnih, V.; Kavukcuoglu, K.; Silver, D.; Graves, A.; Antonoglou, I.; Wierstra, D.; and Riedmiller, M. 2013. Playing atari with deep reinforcement learning. *arXiv preprint arXiv:1312.5602*.
- Mnih, V.; Kavukcuoglu, K.; Silver, D.; Rusu, A. A.; Veness, J.; Bellemare, M. G.; Graves, A.; Riedmiller, M.; Fidjeland, A. K.; Ostrovski, G.; Petersen, S.; Beattie, C.; Sadik, A.; Antonoglou, I.; King, H.; Kumaran, D.; Wierstra, D.; Legg, S.; and Hassabis, D. 2015. Human-level control through deep reinforcement learning. *Nature*, 518(7540): 529–533.
- Narvekar, S.; and Stone, P. 2020. Generalizing curricula for reinforcement learning. In *4th Lifelong Machine Learning Workshop at ICML 2020*.
- Ng, A.; Harada, D.; and Russell, S. J. 1999a. Policy Invariance Under Reward Transformations: Theory and Application to Reward Shaping. In *International Conference on Machine Learning*.
- Ng, A. Y.; Harada, D.; and Russell, S. 1999b. Policy invariance under reward transformations: Theory and application to reward shaping. In *icml*, volume 99, 278–287. Citeseer.
- Oudeyer, P.-Y.; and Smith, L. B. 2016. How evolution may work through curiosity-driven developmental process. *Topics in Cognitive Science*, 8(2): 492–502.
- Papoudakis, G.; Christianos, F.; Schäfer, L.; and Albrecht, S. V. 2021. Benchmarking Multi-Agent Deep Reinforcement Learning Algorithms in Cooperative Tasks. In *Thirty-fifth Conference on Neural Information Processing Systems Datasets and Benchmarks Track (Round 1)*.
- Park, J.; Park, K.; Oh, H.; Lee, G.; Lee, M.; Lee, Y.; and Zhang, B.-T. 2021. Toddler-Guidance Learning: Impacts of Critical Period on Multimodal AI Agents. In *Proceedings of the 2021 International Conference on Multimodal Interaction*, 212–220.
- Pathak, D.; Agrawal, P.; Efros, A. A.; and Darrell, T. 2017. Curiosity-driven exploration by self-supervised prediction. In *International conference on machine learning*, 2778–2787. PMLR.
- Piaget, J.; Cook, M.; et al. 1952. *The origins of intelligence in children*, volume 8. International Universities Press New York.
- Qin, L.; Yan, R.; and Tang, H. 2022. A Low Latency Adaptive Coding Spiking Framework for Deep Reinforcement Learning. *arXiv preprint arXiv:2211.11760*.
- Schulman, J.; Wolski, F.; Dhariwal, P.; Radford, A.; and Klimov, O. 2017. Proximal policy optimization algorithms. *arXiv preprint arXiv:1707.06347*.
- Shonkoff, J.; and Phillips, D. 2000. From Neurons to Neighborhoods: The Science of Early Childhood Development. eric. ed. gov. *National Academy of Sciences Press: Washington DC*. Accessed on May, 8: 2015.
- Taylor, M. E.; and Stone, P. 2009. Transfer learning for reinforcement learning domains: A survey. *Journal of Machine Learning Research*, 10(7).
- Todorov, E.; Erez, T.; and Tassa, Y. 2012. Mujoco: A physics engine for model-based control. In *2012 IEEE/RSJ international conference on intelligent robots and systems*, 5026–5033. IEEE.
- Turchetta, M.; Kolobov, A.; Shah, S.; Krause, A.; and Agarwal, A. 2020. Safe reinforcement learning via curriculum induction. *Advances in Neural Information Processing Systems*, 33: 12151–12162.
- Weinshall, D.; Cohen, G.; and Amir, D. 2018. Curriculum learning by transfer learning: Theory and experiments with deep networks. In *International Conference on Machine Learning*, 5238–5246. PMLR.
- Zhang, B.-T. 1994. Selecting a Critical Subset of Given Examples during Learning. In *International Conference on Artificial Neural Networks*, 517–520. Springer.
- Zhang, D.; Zhang, T.; Jia, S.; Wang, Q.; and Xu, B. 2022a. Tuning Synaptic Connections instead of Weights by Genetic Algorithm in Spiking Policy Network. *arXiv preprint arXiv:2301.10292*.
- Zhang, D.; Zhang, T.; Jia, S.; and Xu, B. 2022b. Multi-scale dynamic coding improved spiking actor network for reinforcement learning. In *Proceedings of the AAAI Conference on Artificial Intelligence*, volume 36, 59–67.

Appendix.

Unveiling the Significance of Toddler-Inspired Reward Transition in Goal-Oriented Reinforcement Learning

- **Section A:** This section provides further details about the experiments conducted in the main text and the appendices.
- **Section B:** This section presents comprehensive results of visualizing the 3D policy loss landscape after the stage-transition for Toddler-inspired S2D Reward Transition and various baselines, which is related to the section: Visualizing Post-Transition 3D Policy Loss Landscape: Cross-Density Visualizer in the main text.
- **Section C:** This section features additional experiments and analyses, as well as further visualizations of the 3D policy loss landscape for various algorithms in the gridworld.

Section A: Experimental Details

A.1 Comparison of Overall Experimental Setup

Table 3: An overall comparison of experimental environments. Those above the double line relate to environments from the main text, while those below correspond to those in the appendices. Each environment and reward was modified to adapt to our experiments for Toddler-inspired S2D reward transition, with details provided in the respective environment setup descriptions.

Environment	Task # of Stages	Difficulty Settings Point of View	Environments Type Action Space	Input Observation Types
OpenAI Gym(Todorov, Erez, and Tassa 2012)	LunarLander-V2 2-stage	- Allocentric View	2D Continuous	Coordinate & Velocity & Angle & Boolean flag value State-based RL
MuJoCo(Todorov, Erez, and Tassa 2012)	CartPole-Reacher 2-stage	- Allocentric View	3D Continuous	Joint Value & Goal Position State-based RL
MuJoCo(Todorov, Erez, and Tassa 2012)	UR5-Reacher 2-stage	- Allocentric View	3D Continuous	Joint Value & Goal Position State-based RL
ViZDoom(Kempka et al. 2016)	Seen & Unseen 2-stage	- Egocentric View	3D Discrete	RGB-D Visual RL
RWARE(Papoudakis et al. 2021)	Shelf-delivery Non-humanoid	Level3 Allocentric View	2D Discrete	Internal state of the surrounding tiles 3-stage & State-based RL
ViZDoom(Kempka et al. 2016)	Obstacles 3-stage	Level3 Egocentric View	3D Discrete	RGB-D Visual RL
Gridworld	Navigation 2-stage	- Allocentric View	2D Discrete	Position-based value State-based RL

Table 4: Detailed settings for hyperparameter N . N is the number of frames of training for the environment after which the stage transition occurs for the respective transition setting (\mathcal{C}_1 , \mathcal{C}_2 , and \mathcal{C}_3). In case of ViZDoom experiments, N indicates the number of updates. For Gridworld-DQN, $\mathcal{C}_1=100$, $\mathcal{C}_2=200$, and $\mathcal{C}_3=300$ episodes.

Environment	Total # of Train	$1N(\mathcal{C}_1)$	$2N(\mathcal{C}_2)$	$3N(\mathcal{C}_3)$
LunarLander-V2	1M frames	100k	200k	400k
ViZDoom-Seen & Unseen	1M frames	50k	100k	250k
CartPole-Reacher	12k episodes	1k	2k	3k
UR5-Reacher	25k episodes	1k	2k	3k
RWARE	7M frames	1M	2M	3M
ViZDoom-FourObj	7M frames	1M	2M	3M
Gridworld	25k episodes	3k	5k	7k

A.2 Reward Transition Hyperparameters

In Table 4 and Figure 7, we have documented the specific point at which the agent transitioned to dense reward stages for each environment with a number of stages.

A.3 Model Hyperparameters

The Table 5 provides information on the hyperparameters for each environment used in our study.

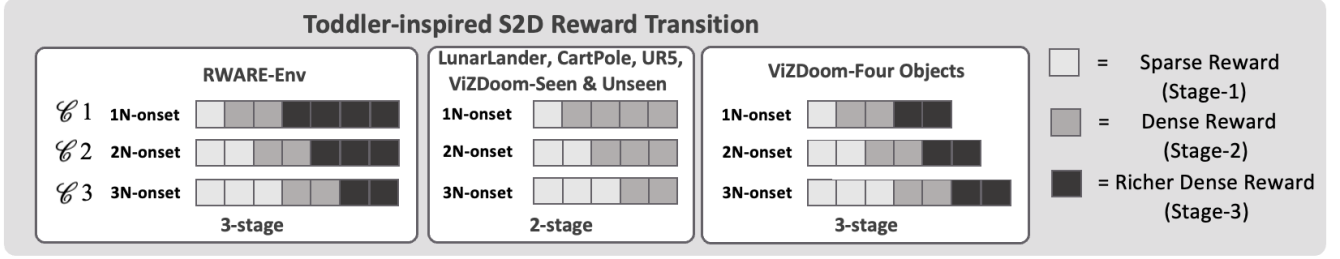


Figure 7: Visualization of the overall setup, including the number of stages and the transition times, in Toddler-inspired S2D experiments across all environments.

Table 5: Hyperparameters for our various experiments for Figure 4 and Appendices. For visualizing the policy loss landscape in LunarLander, we employed discount factors γ of both 1 and 0.99.

Hyperparameters	LunarLander	CartPole-Reacher	UR5-Reacher	ViZDoom-S&U	RWARE	ViZDoom-FourObj	Gridworld
RL algorithms	SAC	SAC	SAC	A3C	PPO	A3C	PPO
Learning Rate	3e-4	0.0007	0.0007	7e-5	5e-4	7e-5	5e-4
Value Function Coefficient	3e-4	-	-	0.5	-	0.5	5e-4
Discount Factor	0.99	0.99	0.99	1.0	0.99	0.99	0.99
Batch Size	128	128	128	-	10	-	128
Optimizer	Adam	Adam	Adam	Adam	Adam	Adam	Adam
Maximum # of Steps	500	200	500	50	150	25	50
Entropy Coefficient	0.2	Auto	Auto	0.1	0.01	0.01	0.03

A.4 Environment Details

All reward-driven baselines and S2D reward were run with more than 4 random seeds for each environment. Our experiments were conducted using four NVIDIA GeForce RTX 3090 GPUs, or two NVIDIA GeForce RTX 2080ti GPUs, with the CPU being an AMD Ryzen Threadripper 3960X 24-Core Processor, and utilizing 188GB of RAM.

Design of sparse to potential-based dense reward. In a sparse-to-dense curriculum, an agent is eventually trained in a dense environment. Here, if a dense reward is not properly defined, the optimal agent in the dense environment may not be optimal in the base (sparse) environment. Therefore, an additional reward in the dense environment must be defined properly so that policy optimality is preserved. In order for optimality to be preserved, we utilize potential-based reward shaping (PBRS) (Ng, Harada, and Russell 1999a; Harutyunyan et al. 2015). In PBRS, an additional reward is given as follows:¹

$$F_i(s, a) = \mathbb{E}_{s' \sim \mathcal{P}(s, a)} [\gamma \Phi_i(s') - \Phi_i(s)], \quad (4)$$

where $\Phi_i : \mathcal{S} \rightarrow \mathbb{R}$ is an arbitrary function called a *potential function* at stage i .

By utilizing the additional reward function F_i , optimality of the policy is preserved, *i.e.*, optimal policy π^* with respect to reward function $\mathcal{R}_i + F_i$ is still optimal with respect to \mathcal{R}_i , as indicated below (Harutyunyan et al. 2015). We note that $\mathcal{R}_i + F_i$ gives a denser reward than \mathcal{R}_i .

$$\begin{aligned} Q(s, a) &= \mathbb{E}_{\mathcal{P}, \pi} \left[\sum_{t=0}^{\infty} \gamma^t (\mathcal{R}_i^t + F_i^t) \mid s_0 = s \right] \\ &= \mathbb{E}_{\mathcal{P}, \pi} \left[\sum_{t=0}^{\infty} \gamma^t (\mathcal{R}_i^t + \gamma \Phi_i(s_{t+1}) - \Phi_i(s_t)) \mid s_0 = s \right] = \mathbb{E}_{\mathcal{P}, \pi} \left[\sum_{t=0}^{\infty} \gamma^t \mathcal{R}_i^t - \Phi_i(s_0) \right]. \end{aligned}$$

In the sparse reward setting (\mathcal{M}_1), the agent only receives a reward when it successfully reaches the goal within a specific distance threshold. In the dense reward setting ($\mathcal{M}_2, \mathcal{M}_3$), the agent receives a potential-based dense reward in addition to the goal-based reward. The dense reward $\psi(\cdot)$, shown in Equation 5, is determined by the agent’s proximity to the goal, which is measured using a positive value based on the L2-distance between the agent’s current position $s \in \mathcal{S}$ and the goal $g \in \mathcal{G}$:

$$\psi(s) = \text{diam}(\mathcal{S}) - \|s - g\|_2, \quad (5)$$

where \mathcal{S} is set of states, $\mathcal{G} \subseteq \mathcal{S}$ is set of goal states, and $\text{diam}(\cdot)$ denotes the diameter of a set.

¹While Φ is the notation commonly used for potential function, we have used ψ throughout our paper.

From a potential-based reward shaping perspective, Table 6 showcases the precise formulations for both sparse and dense rewards across various experimental environments, utilizing distance as the pivotal potential function in the reward design.

Table 6: Reward setting formulation in the environments used for the experiments. Each cell indicates the condition at which a respective sparse or dense reward is provided to the agent. The specific reward values are outlined in the text for each task description.

Reward	LunarLander-V2	CartPole-Reacher	UR5	ViZDoom-Seen	ViZDoom-Unseen
Sparse	$\ s - g\ _2 < 1$	$\ s - g\ _2 < 0.02$	$\ s - g\ _2 < 0.02$	$\ s - g\ _2 < 0.0075$	$\ s - g\ _2 < 0.0075$
Dense	$\gamma\psi(s_{t+1}) - \psi(s_t) < 0.3$	$\gamma\psi(s_{t+1}) - \psi(s_t) < 1$	$\gamma\psi(s_{t+1}) - \psi(s_t) < 1$	$\gamma\psi(s_{t+1}) - \psi(s_t) < 0.14$	$\gamma\psi(s_{t+1}) - \psi(s_t) < 0.14$

OpenAI Gym: LunarLander-V2. The lander begins each episode in mid-air, equipped with a random initial velocity and orientation. The primary objective for the agent is to skillfully maneuver the lander’s engines, guiding it to touch down between the two flags. Ideally, this landing should be at the center of the pad, as vertically aligned as possible, and with minimal speed to ensure a gentle touchdown. Rewards are granted for skillful approaches: transitioning from the screen’s top to the landing pad, achieving a gentle landing with minimal speed, and for each leg that makes ground contact. Conversely, penalties apply for excessive main engine use, encouraging fuel conservation, and significant penalties are incurred for crashes or landing far from the intended pad. For our experiments, we employed the environment’s default rewards as the sparse reward structure and incorporated distance-based, potential-driven dense rewards as part of our Toddler-inspired S2D reward transition, detailed in the above design of reward transition.

Moreover, the potential-based reward shaping we introduced is rooted in a distance-based potential function. Unlike other goal-conditioned environments, in the LunarLander scenario, there is a possibility of receiving rewards for landing at any point on the ground. As such, when the lander approaches within a distance of 0.3 from the ground (where 1.0 indicates the entire screen height), as seen in Table 6, an additional potential-based reward per frame is granted.

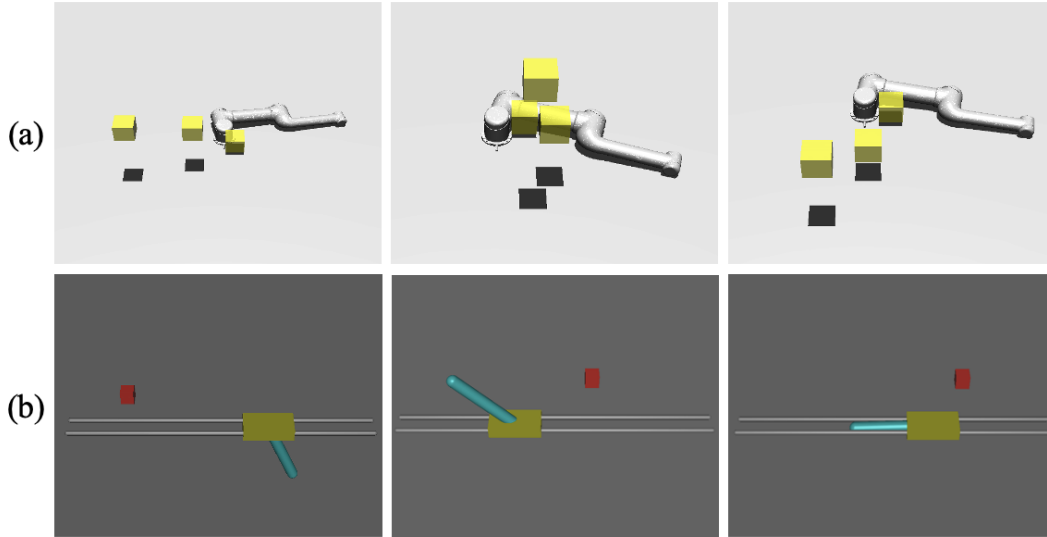


Figure 8: Examples of environments where goals randomly spawn. (a) UR5-Reacher. (b) CartPole-Reacher.

MuJoCo: CartPole-Reacher & UR5-Reacher tasks. To evaluate and compare the effectiveness of Toddler-inspired S2D reward transition in a variety of tasks, we used MuJoCo (Todorov, Erez, and Tassa 2012) engine, a widely used physics engine to simulate manipulation in virtual physical environments. Experiments were conducted in challenging continuous control tasks where a goal is randomly given each episode, and the agent must reach the goal.

CartPole-Reacher is a task where an agent moves the cart along the horizontal line to make the connected pole stand for as long time as possible. Since the agent easily reaches the highest performance in the default task, we made it more challenging by setting a goal that the end of the pole must be within a radius less than a specific threshold. The goal is sampled in the upper side of the horizontal line where it is possible to reach the pole as seen in Figure 8-(b).

UR5-Reacher is a six-degree-of-freedom arm with six joints that each allow movement along one degree of freedom. This flexibility enables the arm to reach a large number of positions and orientations but also makes controlling the arm a challenging

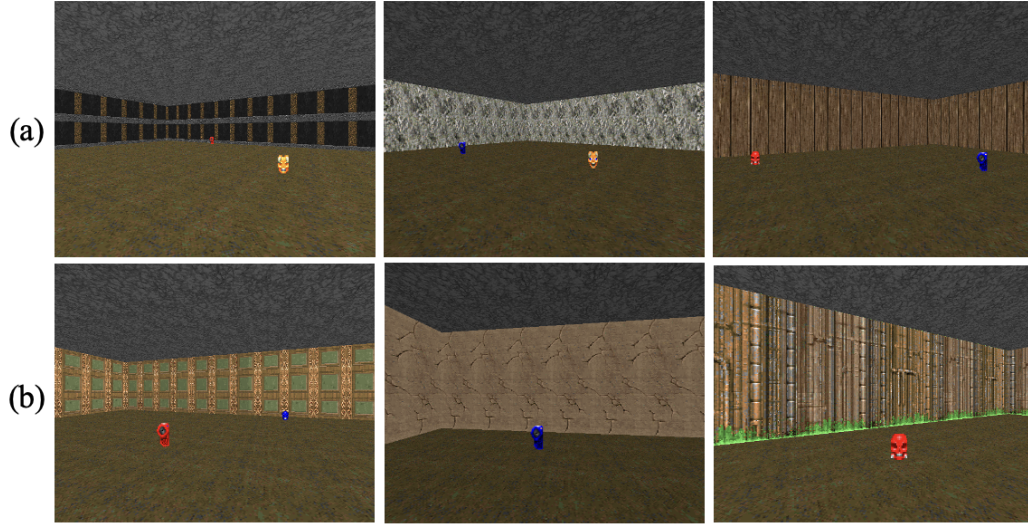


Figure 9: Egocentric views of a ViZDoom agent in environments with various walls and objects. (a) Three walls in ViZDoom-Seen. (b) Three walls in ViZDoom-Unseen.

task. The UR5-Reacher is often simulated as an environment where an agent must learn to control the arm. In our task, the agent needs to learn how to move the arm to a specific position. Our designed goal is randomly spawned for every episode, as seen in Figure 8-(a).

For both UR5-Reacher and CartPole-Reacher, from the very beginning, potential-based dense reward is given based on the distance between the current state of the agent and the goal state as seen in Table 6. Also, a constant time penalty is provided to encourage the agents to solve the tasks quickly.

ViZDoom-Seen & Unseen. ViZDoom (Kempka et al. 2016) is a simulator, based on the first-person shooter game Doom, that was developed to accelerate the reinforcement learning research. In particular, we adopt and modify the egocentric navigation task designed by (Kim et al. 2021), where the agent is placed in one corner of the square room at the start of the episode and must navigate to the correct object out of the two objects spawned in the room. The correct “goal” object is specified every episode uniformly at random, which is known to the agent. The two objects spawned are *Card* and *Skull*, each of them appearing as one of three color variants (Red, Blue, Yellow). This prevents the agent from merely memorizing the objects’ appearances according to their colors. In addition, three wall textures are used in each of Seen and Unseen versions, and these two sets of wall textures are mutually exclusive.

The agent receives a concatenation of 4 frames of RGB-D vision input. Each vision channel has width and height of 42 and 42. The agent can choose among 3 discrete actions: turning clockwise, turning counterclockwise, and moving forward. A single chosen action is repeated for 4 in-game frames. Our manuscript refers to a single “step” within this environment as these 4 consecutive steps.

As a sparse reward function, the agent receives a reward of 10 for arriving at the goal object, and a reward of -1 for arriving at the incorrect object. Reaching either of these objects terminates the episode, which otherwise ends after 50 steps and grants a negative reward of -0.1. For accelerating the training, a negative reward of -0.01 is provided every time step. To render this task visually complex, as well as to evaluate generalization of the trained agent, we use **Seen** and **Unseen** versions of the map as shown in Figure 9 that differ in the set of wall textures used. Dense reward is designed as an additional potential reward of 5.0 provided when the agent arrives within distance of 100 from the goal object. Note that the map size is 700 by 700.

As the baseline, we use the A3C algorithm (Mnih et al. 2016) and the architecture implemented by (Kim et al. 2021)² and (Kim et al. 2023a,b). We also note that all ViZDoom experiments were conducted on the two hardware settings. Experiments on unified hardware settings will be further provided.

²<https://github.com/kibeamKim/GACE-GDAN>

Section B: 3D Visualization of the Policy Loss Landscape After Stage Transition

This study visualizes the 3D policy loss landscape after reward transitions from initially sparse or dense reward settings to two versions: one where sparse reward is provided and another where dense reward is provided. This visualization is done within the same parameter space using *Cross-Density Visualizer*. As hyperparameters for Cross-Density Visualizer, the values for α and β in $\hat{\theta} = \theta + \alpha\mathbf{x} + \beta\mathbf{y}$ range from -10 to 10. Consequently, Sparse-to-Dense (S2D) and Sparse-to-Sparse (Only Sparse) constitute one set, while Dense-to-Sparse (D2S) and Dense-to-Dense (Only Dense) make up another set. We observed a more numerous and distinct smoothing effect, especially under the reward transition of Toddler-inspired S2D. This smoothing effect could facilitate the surmounting of local minima, potentially leading to wider minima.

Results. In the Toddler-inspired S2D reward transition, a greater number of noticeable smoothing effects, such as the reduction in the depth of local minima, are observed. This is evident in the blue landscapes of Figures 10, 11, and 12, particularly in the sections below showing sparse-to-sparse and sparse-to-dense visualizations, in contrast to the D2S, Only Dense, and Only Sparse methods.

Based on our observation of reduced local minima depth, we hypothesize that this facilitates escape from local minima, improving generalization performance on wider minima. To test this, we measure the end-of-training convergence of Toddler-inspired S2D’s neural network to wider minima using sharpness metrics and compare it with those of baselines. As shown in Table 1, Toddler-inspired S2D-guided agents converging to wider minima perform better in dynamic environments. This suggests a correlation between the smoothing effect of the local loss landscape and the likelihood of escaping local minima.

B.1 Additional Insights: Visualizing Policy Loss Landscape After Reward Transition

To gain a deeper understanding of how reward transitions influence agent behavior, we visualized the policy loss landscape after transitions. This examination provides a nuanced view into the nature of the model’s optimization landscape, revealing distinct challenges or advantages that can shape continuous learning.

Distinguishing features of LunarLander-V2’s landscape. What sets LunarLander-V2 as seen in Figure 10 apart from other environments is its unique reward distribution. In this environment, actions such as moving from the screen’s top to the landing pad or achieving a resting state provide rewards ranging between 100 and 140 points. Adversely, actions like deviating from the landing pad or causing a crash lead to deductions. We speculate that such a plethora of reward avenues is what renders the agent’s policy loss landscape rounder and more gently sloped, and less peak-ridden compared to the landscapes in other environments.

Pronounced peaks in CartPole-Reacher and UR5-Reacher. In contrast, the CartPole-Reacher and UR5-Reacher environments exhibit a more singular reward paradigm. Rewards are focused and localized, leading to their policy loss landscapes showcasing distinct peaks, as shown in Figure 11 and 12 for CartPole-Reacher, and UR5-Reacher. This is indicative of the few specific scenarios where agents earn positive feedback.

Through these visualizations, we not only discern the distinct reward mechanisms inherent to different environments but also appreciate how such structures sculpt the policy loss landscapes, influencing agent learning trajectories post-transition.

B.2 Detailed 3D Visualizations for All Baselines

LunarLander-V2: Dense-to-Sparse (D2S) & Dense-to-Dense / Sparse-to-Dense (S2D) & Sparse-to-Sparse

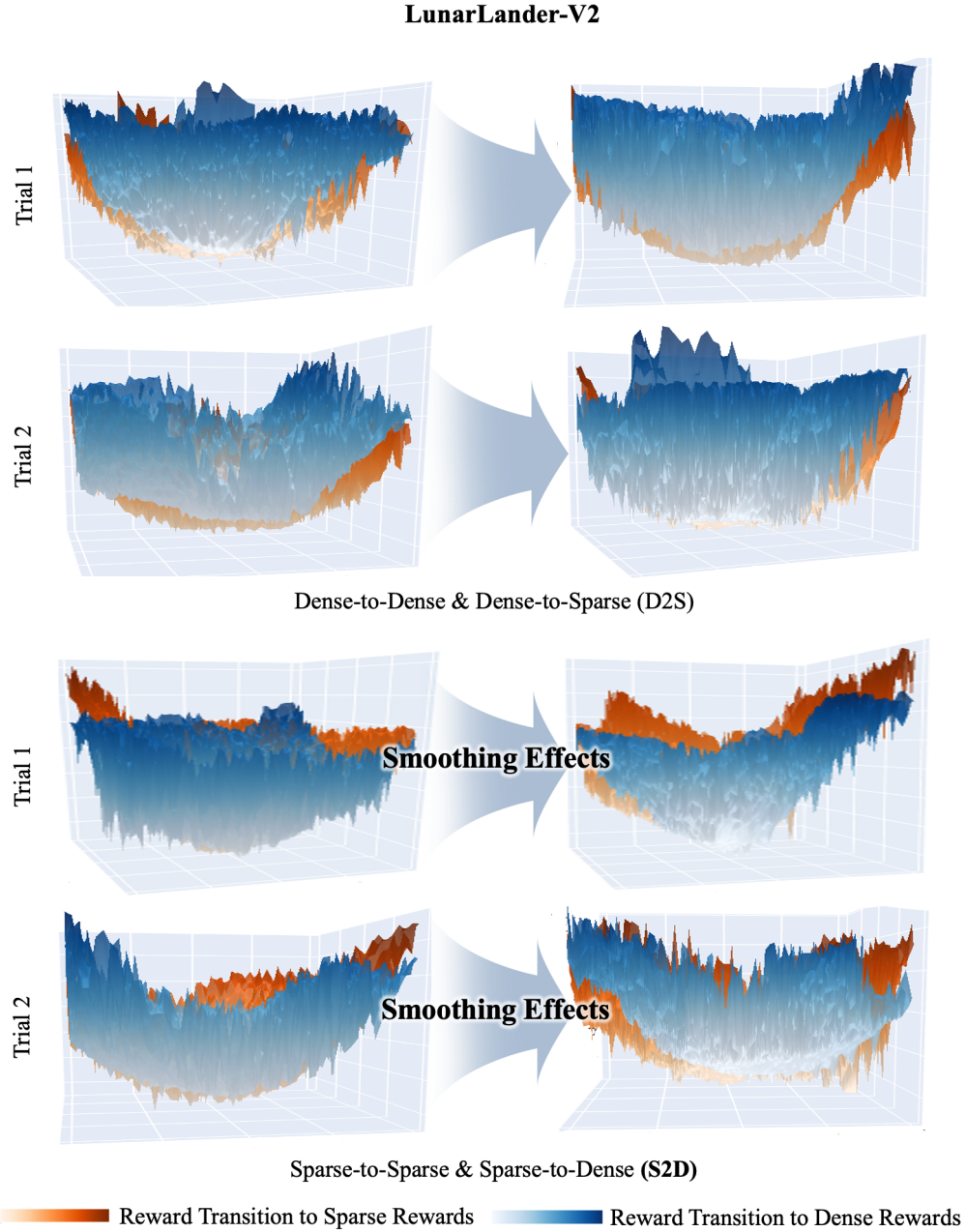


Figure 10: Visualization of the 3D policy loss landscape after reward transitions: The 'low' on the left side illustrates the landscape immediately following the transition, while the 'low' on the right side depicts the landscape around $t = 2000$ after the transition. The first two lines represent dense-to-sparse (D2S, \mathcal{C}_1 , red) and dense-to-dense (Only Dense, blue) transitions. In contrast, the second set of lines represent sparse-to-dense (Toddler-inspired S2D, \mathcal{C}_2 , blue) and sparse-to-sparse (Only Sparse, red) transitions. Notably, the depth of local minima reduction (smoothing effects) is more pronounced under the Toddler-inspired S2D, observed across multiple update points after the reward transition.

CartPole-Reacher: Dense-to-Sparse (D2S) & Dense-to-Dense / Sparse-to-Dense (S2D) & Sparse-to-Sparse

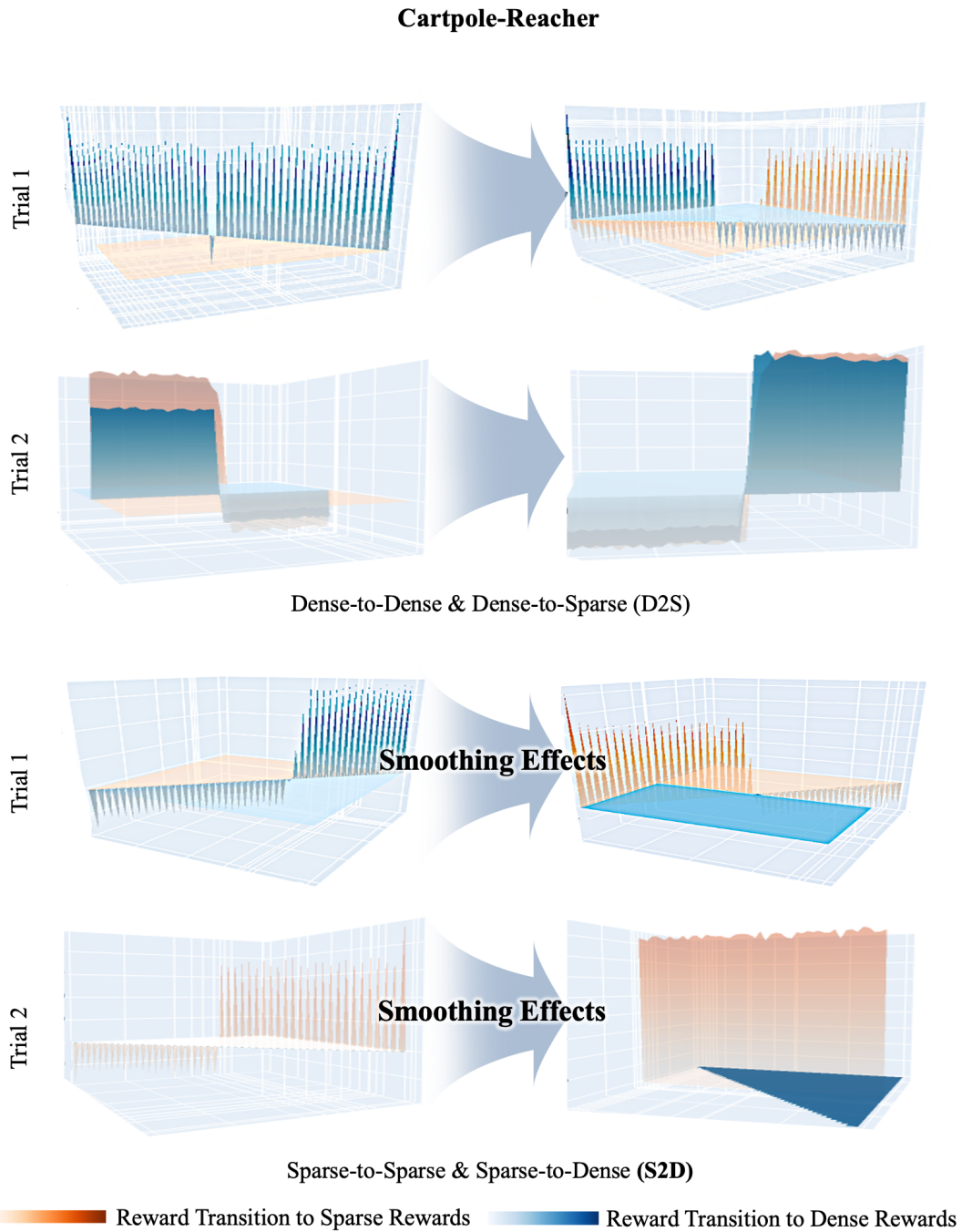


Figure 11: In the visualization of the 3D policy loss landscape after reward transitions, significant smoothing effects were more frequently observed when applying the Toddler-inspired S2D (sparse-to-dense, \mathcal{C}_2 , blue) reward transition.

UR5-Reacher: : Dense-to-Sparse (D2S) & Dense-to-Dense / Sparse-to-Dense (S2D) & Sparse-to-Sparse

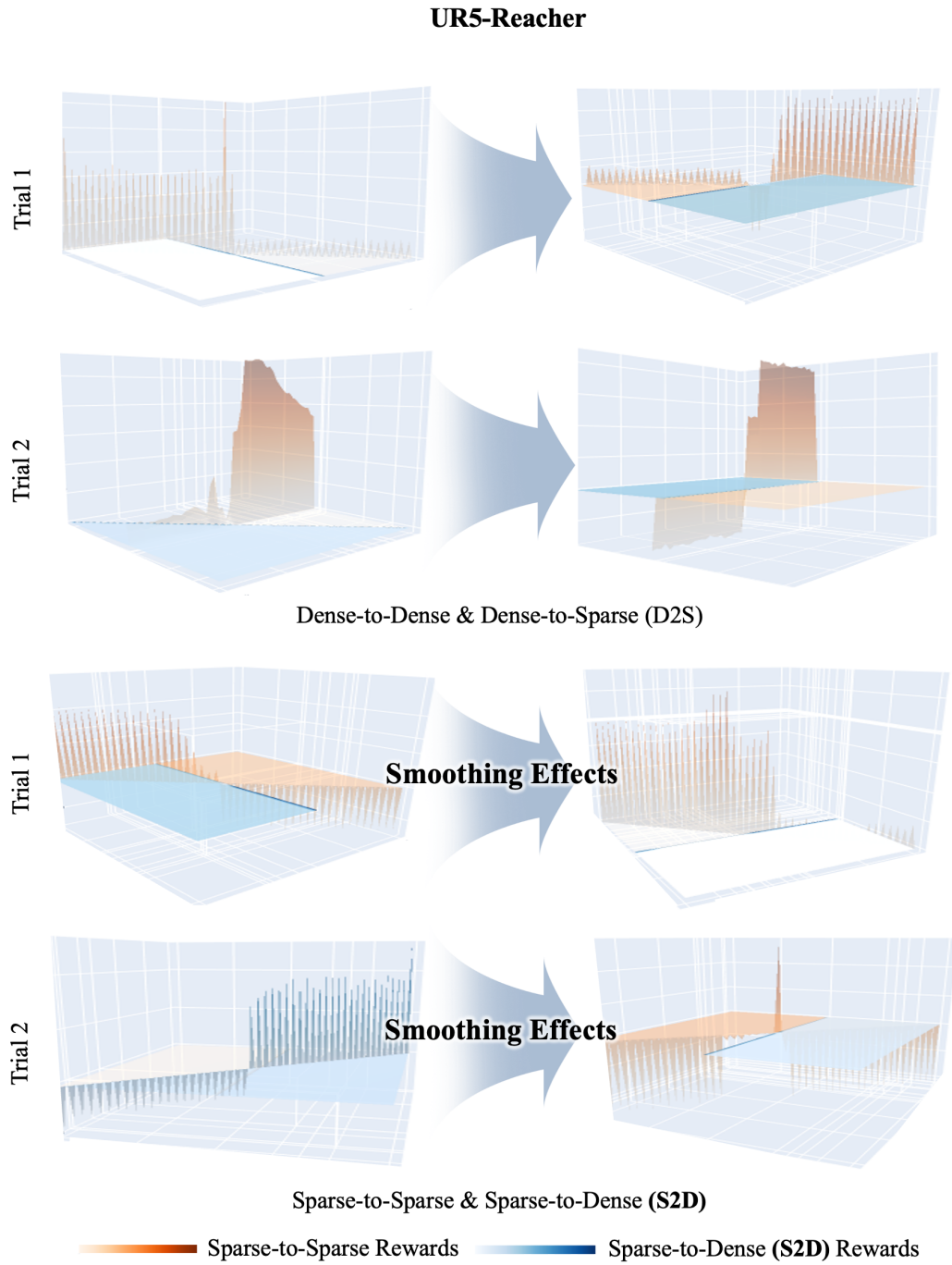


Figure 12: Visualization of the 3D policy loss landscape after stage-transitions in sparse-to-dense (Toddler-inspired S2D, \mathcal{C}_3 , blue) and sparse-to-sparse (Only Sparse, red). Here, in the UR5-reacher, the improvement in performance of S2D over only dense becomes apparent later, and until that point, the performance of the two is generally not significantly different. Perhaps because of that, the Only Dense model also often showed a lower depth of local minima depending on the seed immediately after the reward transition. Yet, we observed even more smoothing effects due to the decrease in the depth of local minima under Toddler-inspired S2D reward transition, even compared to other baselines.

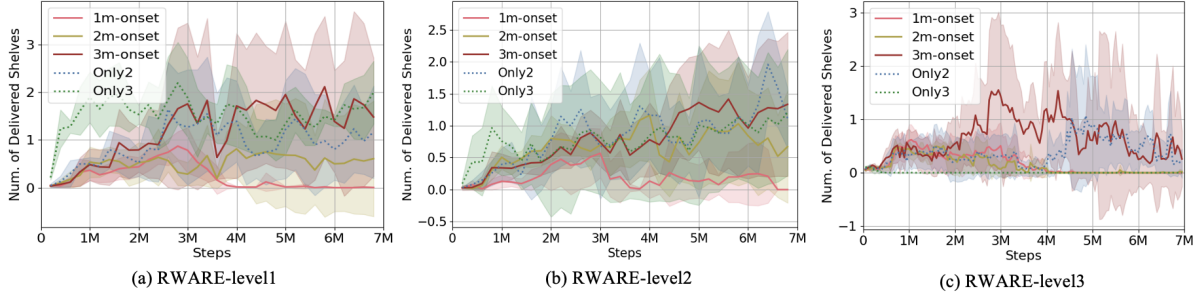


Figure 13: Performance of the agents in RWARE tasks. Vertical axis indicates the average number of requested shelves successfully delivered to the goal per episode. Horizontal axis indicates the number of time steps. The solid lines show the performances of Toddler-inspired S2D reward transition agents (\mathcal{C}_1), (\mathcal{C}_2), and (\mathcal{C}_3), while the dotted lines show the performances of only dense reward agents (\mathcal{C}_4). The mean and standard deviation of each agent in each level across five trials are shown as lines and shaded regions respectively. (\mathcal{C}_3) agent shows one of highest-performing learning curves in the three environments, even when the Stage-3 guidance may be unhelpful as in Level 3. Both the Toddler-inspired S2D reward transition agents and the only dense reward agents show substantial standard deviation, which we claim is due to the difficulty of these RWARE tasks, which involve subgoals.

Section C: Additional Experiments of Toddler-Inspired S2D Reward Transition in Various Environments

C.1 Shelf Delivery Tasks on RWARE: Experiments on Suboptimal Reward Structure

Task settings. As seen in Figure 13 and 14, We conduct additional experiments on grid-world RWARE environments with discrete state-action space. Modified from RWARE (Papoudakis et al. 2021) to be a single-agent setting, each environment contains a mobile agent and several rows of shelves (blue), some of which are randomly sampled and “requested” (red) to be delivered. The agent has an available action space of $\{\text{MoveForward}, \text{TurnLeft}, \text{TurnRight}, \text{Load/Unload}, \text{Noop}\}$. The agent observes only the information of tiles within 3-by-3 square area centered at the agent. The agent must carry and deliver requested shelves to the goal location (green). This can be deemed as a task with subgoals, where the agent must first reach the tile with the requested shelf, pick up the shelf and carry it to the goal, and then return the shelf back to its original position.

We designate separate environmental settings for three difficulty settings: Level1 contains 8 shelves, 3 of which are requested; Level2 contains 10 shelves, 3 of which are requested, leading to sparser reward; Level3 is a vast environment with a total of 32 shelves, 16 of which are requested. The space to explore is magnified as the difficulty increases. These environments are illustrated in Figure 14.

Design of guidance. Reward functions for three different stages of guidance are naturally designed according to this sequence of subtasks: Stage-1 guidance provides +1.0 reward when the agent successfully carries a requested shelf to a goal location; Stage-2 guidance provides reward for the delivery and returning the shelf to its original location; Stage-3 guidance provides an additional reward for picking up a requested shelf.

Results on RWARE environments. The purpose of this study is to examine the effect of different Toddler-inspired S2D reward transition on learning the tasks in RWARE that involve a sequence of *subgoals* in order to clearly observe the sub-optimal situation following the Toddler-inspired S2D models near the transition times. The experiments investigated the Toddler-inspired S2D reward transition models at the timing of three different stage transitions (\mathcal{C}_1 , \mathcal{C}_2 , and \mathcal{C}_3), as well as only dense reward applied to learn with only Stage-2 (\mathcal{C}_4) or Stage-3 (\mathcal{C}_5) guidance provided. The transition times are the same as specified for ViZDoom-FourObjects in Figure 7, with N set to 1M time steps. PPO (Schulman et al. 2017) was used as the RL algorithm, and the means and standard deviations were recorded across five trials. We analyze the results below:

- **Level1.** (Figure 13-(a)). Among the Toddler-inspired S2D reward transition agents, the \mathcal{C}_3 agent performs the best, while the \mathcal{C}_1 agent fails to deliver any shelves after the 4M time step. While the Only 2 (\mathcal{C}_4) and Only 3 (\mathcal{C}_5) agents achieve remarkable performances, \mathcal{C}_3 agent performs on par with, if not better than, these only dense reward agents.
- **Level2.** (Figure 13-(b)). Similarly to the results in Level-1, the \mathcal{C}_3 agent performs the best, followed by \mathcal{C}_2 agent. The Only 2 (\mathcal{C}_4) and Only 3 (\mathcal{C}_5) agents achieve performances similar to that of \mathcal{C}_3 agent in this problem as well.
- **Level3.** (Figure 13-(c)). The \mathcal{C}_3 agent achieves the top performance in this most difficult setting. It should be noted that, despite our original intent, the Stage-3 guidance was not beneficial in learning to solve the task, as indicated by the performance of Only 3 agent (\mathcal{C}_4). Nevertheless, \mathcal{C}_3 agent showed the greatest robustness to such detrimental reward.

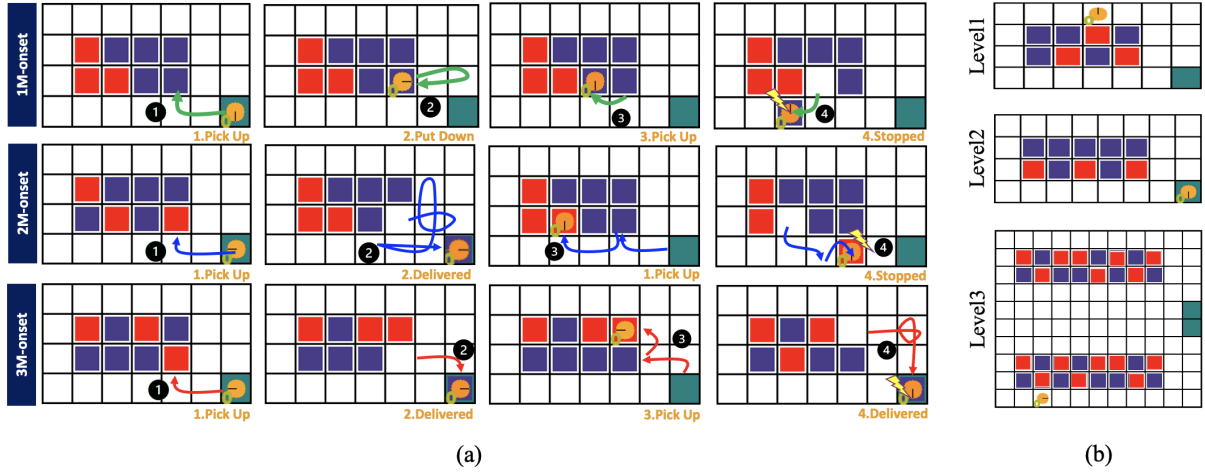


Figure 14: (a) Visualization of the trajectory for each agent policy in RWARE-Level1. (b) Three levels of RWARE environments.

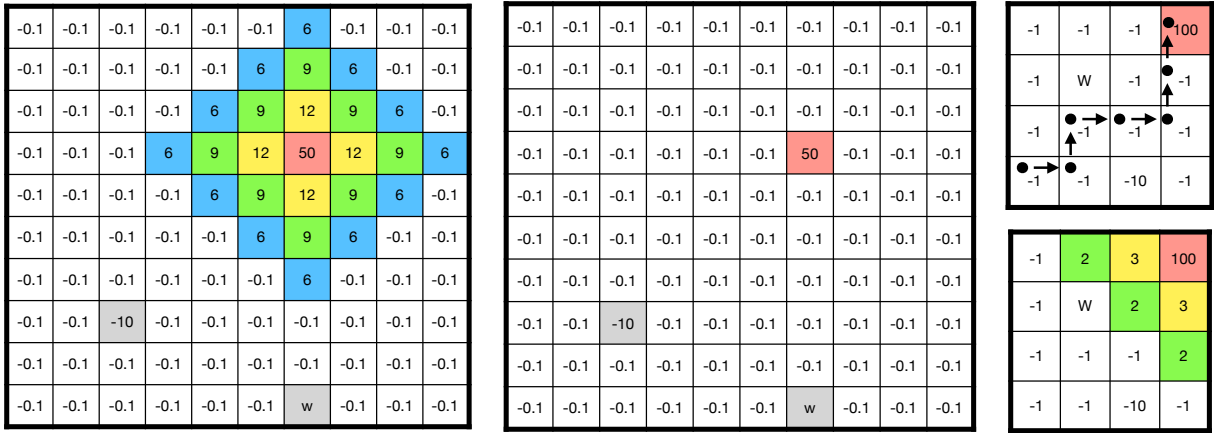


Figure 15: Gridworld-navigation task. **Left:** Potential-based dense reward environment of 10×10 with *PPO*. **Center:** sparse reward environment of 10×10 with *PPO*. **Right-Top:** sparse reward environment of 4×4 with *DQN*. **Right-Bottom:** Potential-based dense reward environment of 4×4 with *DQN*.

Overall analysis on RWARE environments. In Figure 14, we illustrate the policy trajectories of various agents in RWARE-Level1. The goal, requested shelves, and non-requested shelves are marked as green, red, and blue squares respectively. Here, the starting point of the agent is the same as the goal position (green). The \mathcal{C}_1 agent picks incorrect shelves twice, and then halts exploration. The \mathcal{C}_2 agent initially picks the correct shelf and delivers it, but inefficiently explores the destination area in subsequent attempts. Unlike these two agents, the \mathcal{C}_3 agent delivers more shelves efficiently and experiences fewer subgoal failures. This, similarly to the observation in ViZDoom-FourObjects experiments, highlights the impact of reward transition times on task performance.

Importance of early free exploration. We also observe that the \mathcal{C}_1 and \mathcal{C}_2 agents perform poorly when the first stage transition is given early, before the point of 3M training steps, as seen in Figure 13. Therefore, we believe that a proper amount of exploration stage (Stage-1) given sparse reward is essential to successful learning. For Only 3 agent (\mathcal{C}_5), even with the richest reward, the agent fails completely in Level3. However, we found that our \mathcal{C}_3 agent is even robust to the unbeneficial reward through first stage transition in Toddler-inspired S2D setting.

C.2 Gridworld: Add-on Algorithms Experiments on 3D Loss Landscape

We conducted 3D visualization of the policy landscape and experiments on performance in the Gridworld environment, which we selected due to its relative simplicity and minimal environmental factors. This setup provided a more straightforward context in which to observe the results according to both the S2D reward transition and the baseline, thereby offering clearer insights into the implications of our work. In the main text, we focused solely on visualizing the policy loss landscape using the SAC

algorithm (Haarnoja et al. 2018). To verify whether the smoothing effects still persist in other various algorithms, we conducted additional experiments using the DQN (Mnih et al. 2015) and PPO (Schulman et al. 2017).

Environment setup. The experimental environment is a gridworld, as shown in Figure 15. The agent can perform actions of moving in four directions: up, down, left, and right. It receives a living penalty of -0.1 to encourage exploration. The experiment is conducted under two environment settings: (1) a fixed goal 4×4 environment with DQN (Mnih et al. 2015) and (2) a random goal 10×10 environment with PPO (Schulman et al. 2017). Initially, we found an appropriate stage transition: $T = 200$ for a fixed goal within a total of 1000 steps, and $T = 5000$ for a random goal within a total of 100,000 steps. The neural network used for learning (Mnih et al. 2015; Schulman et al. 2017) consists of three fully connected layers with ReLU activation. The batch size is set to 128. In the case of PPO, we updated every 2 episodes. We employed the Cross-Density Visualizer strategy.

The result of loss landscape in DQN and PPO algorithms. We visualized PPO for the policy loss landscape and DQN for the Q-function loss landscape. This is because, while DQN (Deep Q-Network) primarily aims to learn a Q-value function, observing the Q-value loss landscape can offer valuable insights into the network’s learning dynamics and its adaptability to varied reward schemes. For both gridworld-DQN and PPO, only the Toddler-inspired S2D reward transition exhibits a notable smoothing effect with the highest performance results compared to the other baselines, as depicted in Figures 16, 17, and 18-(b). However, as seen in Figures 17 and 18-(a), we observe little to no difference between the dense and sparse loss landscapes as the number of updates increases. Therefore, we conclude that proceeding in a sparse-to-dense manner, i.e., using Toddler-inspired S2D reward transition, is an effective method for reducing the depth of local minima. It proves to be significantly more effective than the dense-to-sparse (D2S) or Only Dense approach.

C.4 Detailed 3D Loss Landscape Visualizations for Gridworld-PPO and DQN Algorithm

Gridworld-PPO: Sparse-to-Dense (S2D) & Sparse-to-Sparse (Only Sparse)

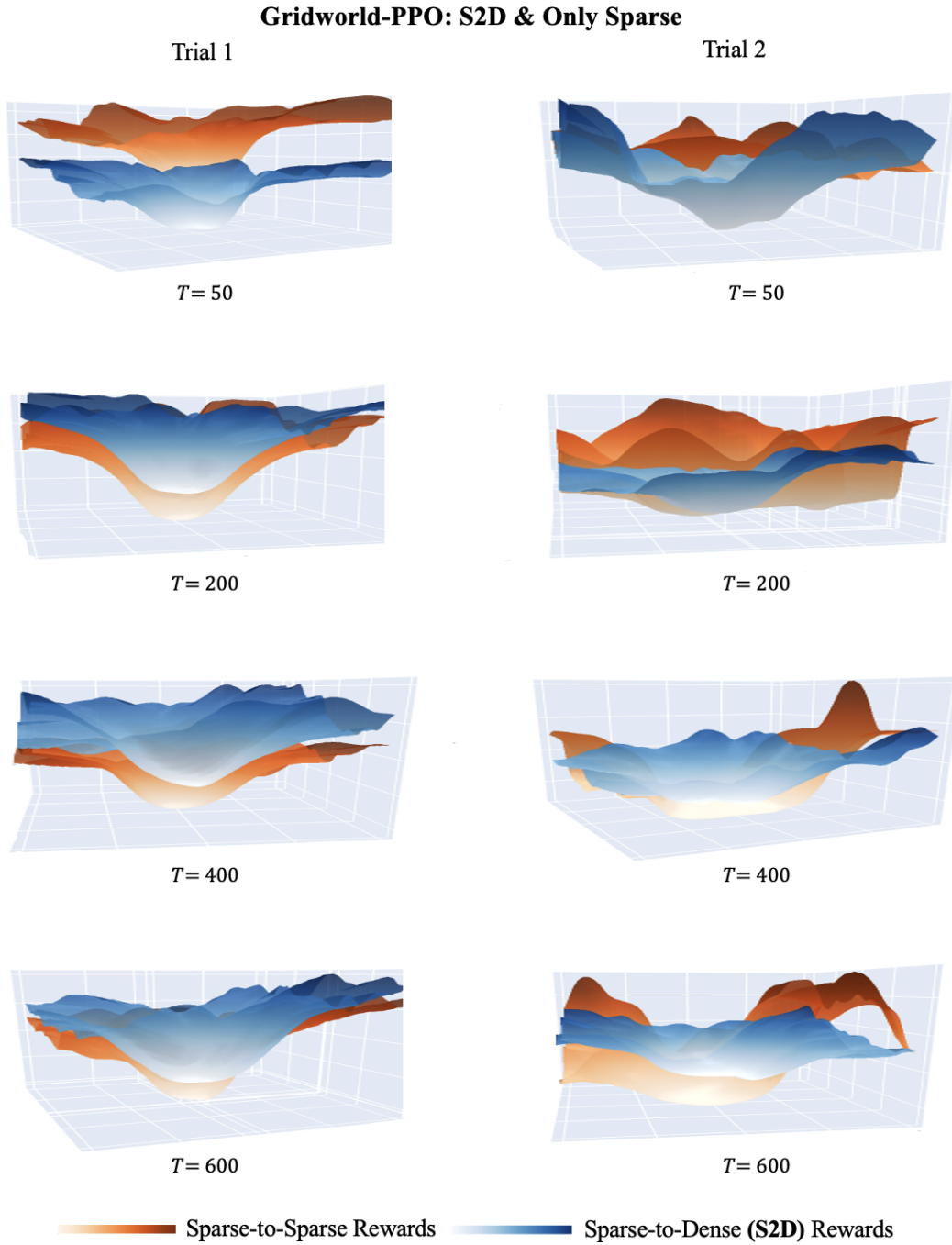


Figure 16: Visualization of the 3D policy loss landscape after stage-transitions in sparse-to-dense (Toddler-inspired S2D, \mathcal{C}_3 , blue) and sparse-to-sparse (Only Sparse, red). Here, we also observed notable smoothing effects (reduction in the depth of local minima) under Toddler-inspired S2D reward transition in PPO algorithm.

Gridworld-PPO: Dense-to-Sparse (D2S) & Dense-to-Dense (Only Dense)

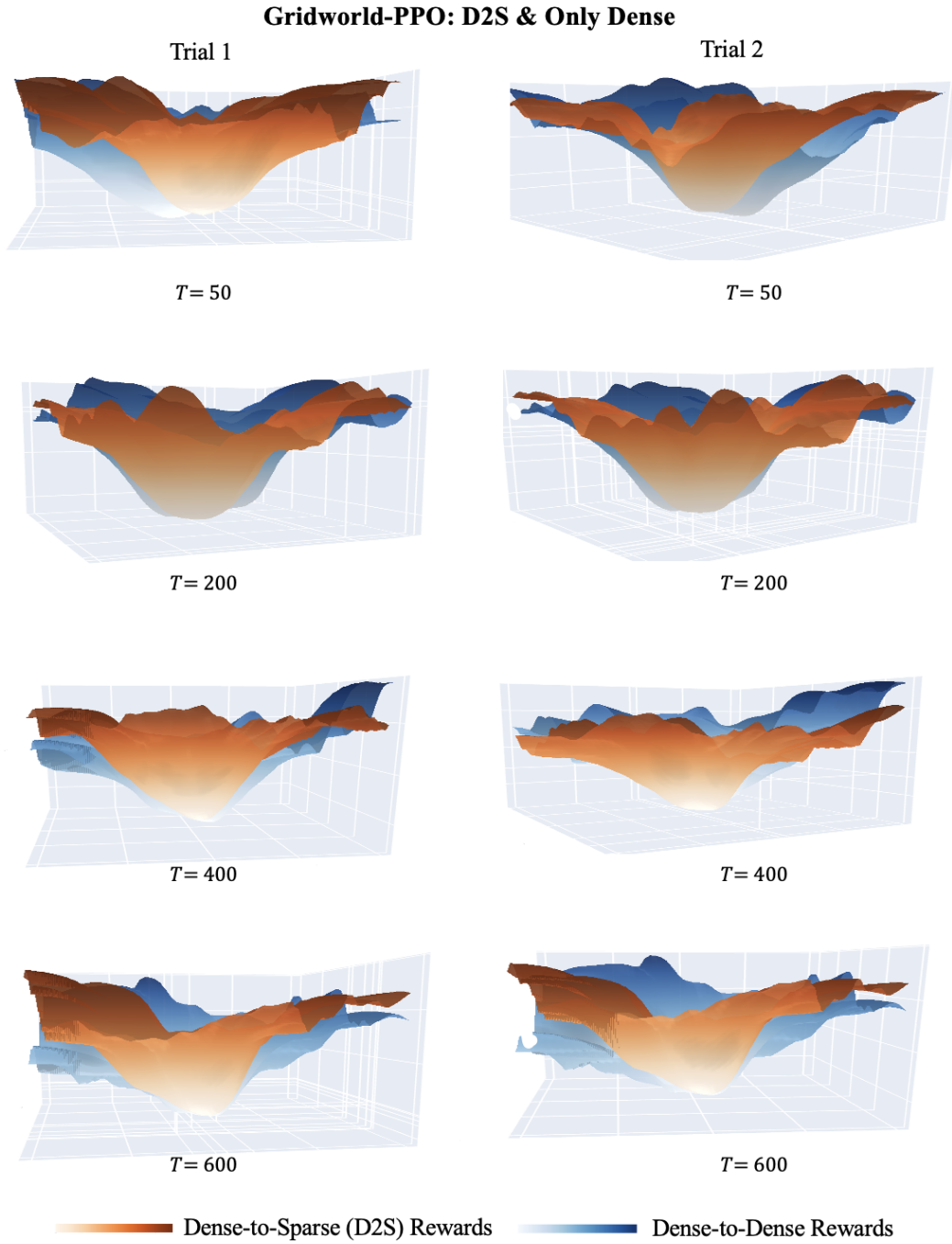


Figure 17: Visualization of the 3D policy loss landscape after stage-transitions in dense-to-sparse (D2S, \mathcal{C}_3 , red) and dense-to-dense (Only Dense, blue). Similar to other D2S and Only Dense results in Appendix Section B, we also cannot observe notable smoothing effects consistent with the number of updates within Gridworld-PPO.

Gridworld-DQN: S2D, Only Sparse & D2S, Only Dense

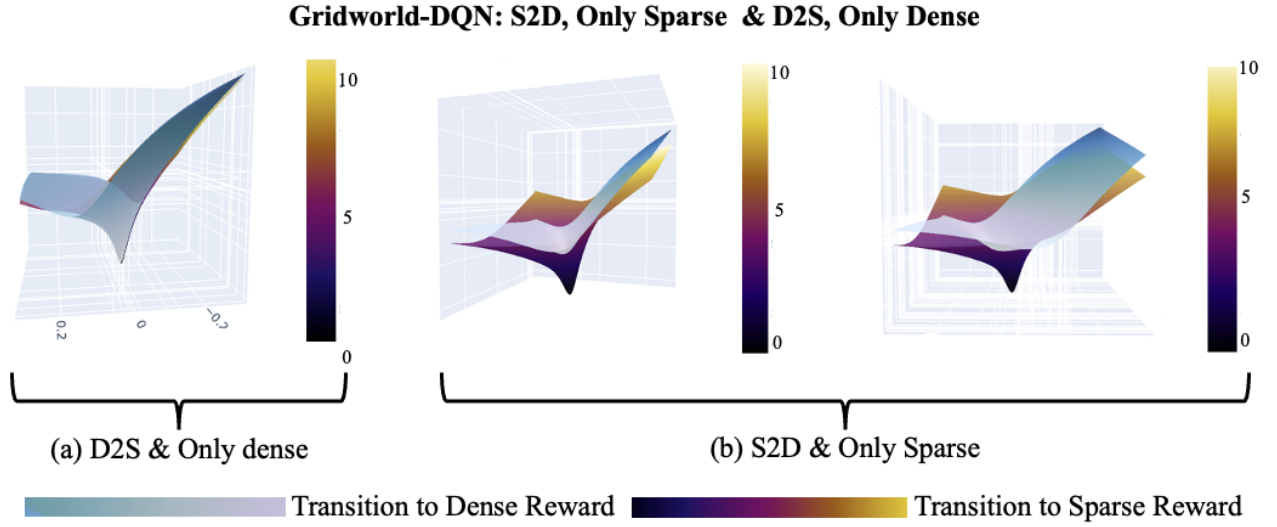


Figure 18: Visualization of the 3D Q-value loss landscape after reward transitions in Toddler-inspired S2D and other baselines. A smoothing effect is not apparent for the baselines (D2S, Only Dense, Only Sparse). However, under [Toddler-inspired S2D](#) reward transition in (b) exclusively, a clear smoothing effect can be observed after transitioning to potential-based dense rewards by reducing the depth of local minima.

Additional Future Works

The approach examined in our research is inspired by the modeling of bio-inspired systems, particularly those based on toddler behaviors. Within this framework, our future research endeavors will focus on a deeper exploration of bio-plausible networks or models. We propose the following areas for future investigation, which we believe are pivotal for advancing our understanding at two critical junctures.

- 1. Reward Transition Patterns in SNN Based RL:** One promising avenue is the utilization of spiking neural networks (SNNs), which offer a more biologically realistic simulation of neural activity. Building upon bio-plausible SNN based RL research (Qin, Yan, and Tang 2022; Zhang et al. 2022b,a), we intend to investigate how SNNs can model and potentially enhance our understanding of reward transition dynamics in RL scenarios. By integrating toddler-inspired approaches into SNN research, we could provide novel insights into how rewards are processed and learned over time in SNN.
- 2. Exploring the Critical Period: Optimal Reward Transition Timing:** Another intriguing aspect is the initial period of free exploration in RL, which is crucial for learning effective strategies in our toddler-inspired reward transition. Through empirical experimentation, we were able to observe that the timing of the reward transition with proper guidance significantly affects subsequent performance and is a crucial parameter. This phenomenon can also be considered similar to the concept of the 'critical period' observed in infants. In human infants, appropriate training or proper guidance in the early stages of learning significantly impacts future learning. Moreover, the importance of suitable early education is evident from research on RL models (Park et al. 2021; De Kleijn, Sen, and Kachergis 2022) and neural networks (Achille, Rovere, and Soatto 2018) regarding this critical period. To advance this research area, our analysis, which includes the smoothing effect and low sharpness metrics of the S2D model, suggests that exploring the optimal timing for reward transition during the initial learning phase presents a promising avenue for future studies.

We hope that our research will contribute to a broader understanding of neural network architectures and their learning mechanisms, bridging the gap between artificial intelligence and biological or cognitive modeling systems.

Pytorch-like Code for Loss Landscape Rendering

Algorithm 1: Perpendicular Random Directions Generation

```
1: rand_direction_list1  $\leftarrow \emptyset$ 
2: rand_direction_list2  $\leftarrow \emptyset$ 
3: for each param in network.parameters() do
4:   r  $\leftarrow$  torch.randn_like(param)
5:   r2  $\leftarrow$  torch.randn_like(param)
6:   r  $\leftarrow$  r -  $\left( \frac{\text{torch.dot}(r.\text{reshape}(-1), r2.\text{reshape}(-1))}{\|r2.\text{reshape}(-1)\|^2} \right) * r2$ 
7:   r  $\leftarrow$   $\left( \frac{r}{\|r\|} \right) * \|param.\text{detach}()\|$ 
8:   r2  $\leftarrow$   $\left( \frac{r2}{\|r2\|} \right) * \|param.\text{detach}()\|$ 
9:   rand_direction_list1.append(torch.nan_to_num(r))
10:  rand_direction_list2.append(torch.nan_to_num(r2))
11: end for
```

Algorithm 2: Deterministic Sampling

```
1: class ReplayBuffer:
2:   def __init__(self, memory_size):
3:     self.memory = deque(maxlen=memory_size)
4:     self.experience = namedtuple("Experience",
5:       field_names=["state", "action", "reward", "next_state", "done", "episode"])
6:     # The rest is the same as a conventional replaybuffer.
7:   def deterministic_sample(self, size):
8:     idx = min(size-1, len(self.memory)-1)
9:     experiences = [self.memory[i] for i in range(len(self.memory)-1-idx, len(self.memory)-1)]
10:
11:     states = np.vstack([e.state for e in experiences if e is not None])
12:     actions = np.vstack([e.action for e in experiences if e is not None])
13:     rewards = np.vstack([e.reward for e in experiences if e is not None])
14:     next_states = np.vstack([e.next_state for e in experiences if e is not None])
15:     dones = np.vstack([e.done for e in experiences if e is not None]).astype(np.bool_)
16:
17:     min_epi = self.memory[0].episode
18:     max_epi = self.memory[idx - 1].episode
19:
20:     return states, actions,
21:       np.squeeze(rewards, axis=1), next_states,
22:       np.squeeze(dones, axis=1)
```

Algorithm 3: Network Base

```
1: class NetworkBase:
2:   def __init__(self):
3:     self.value_net = ValueNetwork(state_dim, hidden_dim)
4:     self.target_value_net = ValueNetwork(state_dim, hidden_dim)
5:
6:     self.soft_q_net1 = SoftQNetwork(state_dim, action_dim, hidden_dim)
7:     self.soft_q_net2 = SoftQNetwork(state_dim, action_dim, hidden_dim)
8:     self.policy_net = PolicyNetwork(state_dim, action_dim, hidden_dim)
```

Algorithm 4: Network Copy

```
1: function REPLICASelf(self)
2:   result  $\leftarrow$  NetworkBase(self.device)
3:   for each target_param, param in zip(result.value_net.parameters(), self.value_net.parameters()) : do
4:     target_param.data.copy_(param.data) ▷ Repeated for all networks.
5:   end for
6:   return result
7: end function
```

Algorithm 5: Loss Landscape Calculation for Policy

```
1: state, action, reward, next_state, done  $\leftarrow$  replay_buffer.deterministic_sample()
2: xs  $\leftarrow$  torch.linspace(-10, 10, steps = 50)
3: ys  $\leftarrow$  torch.linspace(-10, 10, steps = 50)
4: xs, ys  $\leftarrow$  torch.meshgrid(xs, ys, indexing = 'xy')
5: zs  $\leftarrow$  torch.zeros_like(xs)
6: for i in range(xs.shape[0]) do
7:   for j in range(ys.shape[1]) do
8:     new_model  $\leftarrow$  self.replica()
9:     for param, new_param, rand_dir1, rand_dir2 in zip(self.policy_net.parameters(), new_model.policy_net.parameters(), self.r
10:   do
11:     transformed  $\leftarrow$  param + xs[i][j] * rand_dir1 + ys[i][j] * rand_dir2
12:     new_param.copy_(transformed)
13:   end for
14:   new_a, log_prob,  $\epsilon$ , mean, log_std  $\leftarrow$  new_model.policy_net.evaluate(state)
15:   predicted_new_q_value  $\leftarrow$  torch.min(
16:     new_model.soft_q_net1(state, new_a),
17:     new_model.soft_q_net2(state, new_a)
18:   )
19:   zs[i][j]  $\leftarrow$  (log_prob - predicted_new_q_value).mean().item()
20: end for
21: end for
22: return xs.numpy(), ys.numpy(), zs.numpy()
```

Algorithm 6: Cross-Density Visualizer

```
1: dense_agent  $\leftarrow$  NetworkBase(device = device)
2: dense_replay_buffer  $\leftarrow$  ReplayBuffer(replay_buffer_size)
3: for episode in trange(transition_episode) : do
4:   state,  $\_ \leftarrow$  env.reset(seed = seed)
5:   for step in range(max_step) : do
6:     action  $\leftarrow$  env.action_space.sample()
7:     next_state, reward, done,  $\_ , \_$ 
8:       = env.step(action)
9:     reward  $\leftarrow$  dense_reward(next_state, reward)
10:    dense_replay_buffer.push(state, action, reward, next_state, done, episode)
11:    state  $\leftarrow$  next_state
12:    dense_agent.update(dense_replay_buffer)
13:    if done then
14:      break
15:    end if
16:  end for
17:  draw_landscape()
18: end for
19:
20: dense_to_sparse_agent  $\leftarrow$  dense_agent.replica()
21: dense_to_sparse_replay_buffer  $\leftarrow$  copy.deepcopy(dense_replay_buffer)
22: for episode in trange(transition_episode, max_episodes) : do
23:   state,  $\_ \leftarrow$  env.reset(seed = seed)
24:   for step in range(max_step) : do
25:     action  $\leftarrow$  dense_agent.policy_net.get_action(state).detach()
26:     next_state, reward, done,  $\_ , \_$ 
27:       = env.step(action.numpy())
28:     reward  $\leftarrow$  dense_reward(next_state, reward)
29:     dense_replay_buffer.push(state, action, reward, next_state, done, episode)
30:     state  $\leftarrow$  next_state
31:      $\_ \leftarrow$  dense_agent.update(dense_replay_buffer)
32:     if done then
33:       break
34:     end if
35:   end for
36:
37:   state,  $\_ \leftarrow$  env.reset(seed = seed)
38:   for step in range(max_step) : do
39:     action  $\leftarrow$  dense_to_sparse_agent.policy_net.get_action(state).detach()
40:     next_state, reward, done,  $\_ , \_$ 
41:       = env.step(action.numpy())
42:     dense_to_sparse_replay_buffer.push(state, action, reward, next_state, done, episode)
43:     state  $\leftarrow$  next_state
44:      $\_ \leftarrow$  dense_to_sparse_agent.update(dense_to_sparse_replay_buffer)
45:     if done then
46:       break
47:     end if
48:   end for
49:
50:   draw_landscape()
51: end for
```

▷ Cross-Density Running